



2017

THE LIMITS & EFFECTS OF DRAW ON PROPERTIES AND MORPHOLOGY OF PAN-BASED PRECURSOR AND THE RESULTANT CARBON FIBERS

Sarah Edrington

University of Kentucky, sarah.edrington@uky.edu

Digital Object Identifier: <https://doi.org/10.13023/ETD.2017.165>

[Click here to let us know how access to this document benefits you.](#)

Recommended Citation

Edrington, Sarah, "THE LIMITS & EFFECTS OF DRAW ON PROPERTIES AND MORPHOLOGY OF PAN-BASED PRECURSOR AND THE RESULTANT CARBON FIBERS" (2017). *Theses and Dissertations--Mechanical Engineering*. 89. https://uknowledge.uky.edu/me_etds/89

This Master's Thesis is brought to you for free and open access by the Mechanical Engineering at UKnowledge. It has been accepted for inclusion in Theses and Dissertations--Mechanical Engineering by an authorized administrator of UKnowledge. For more information, please contact UKnowledge@lsv.uky.edu.

STUDENT AGREEMENT:

I represent that my thesis or dissertation and abstract are my original work. Proper attribution has been given to all outside sources. I understand that I am solely responsible for obtaining any needed copyright permissions. I have obtained needed written permission statement(s) from the owner(s) of each third-party copyrighted matter to be included in my work, allowing electronic distribution (if such use is not permitted by the fair use doctrine) which will be submitted to UKnowledge as Additional File.

I hereby grant to The University of Kentucky and its agents the irrevocable, non-exclusive, and royalty-free license to archive and make accessible my work in whole or in part in all forms of media, now or hereafter known. I agree that the document mentioned above may be made available immediately for worldwide access unless an embargo applies.

I retain all other ownership rights to the copyright of my work. I also retain the right to use in future works (such as articles or books) all or part of my work. I understand that I am free to register the copyright to my work.

REVIEW, APPROVAL AND ACCEPTANCE

The document mentioned above has been reviewed and accepted by the student's advisor, on behalf of the advisory committee, and by the Director of Graduate Studies (DGS), on behalf of the program; we verify that this is the final, approved version of the student's thesis including all changes required by the advisory committee. The undersigned agree to abide by the statements above.

Sarah Edrington, Student

Dr. Rodney Andrews, Major Professor

Dr. Haluk Karaca, Director of Graduate Studies

THE LIMITS & EFFECTS OF DRAW ON PROPERTIES AND MORPHOLOGY OF
PAN-BASED PRECURSOR AND THE RESULTANT CARBON FIBERS

THESIS

A thesis submitted in partial fulfillment of the
requirements for the degree of Master of Science in Mechanical Engineering
in the College of Engineering
at the University of Kentucky

By

Sarah Edrington

Lexington, Kentucky

Co-Directors: Dr. Rodney Andrews, Professor of Mechanical Engineering
and Dr. Matthew Weisenberger, Adjunct Assistant Professor, Chemical and Materials
Engineering

Lexington, Kentucky

2017

Copyright © Sarah Edrington 2017

ABSTRACT OF THESIS

THE LIMITS & EFFECTS OF DRAW ON PROPERTIES AND MORPHOLOGY OF PAN-BASED PRECURSOR AND THE RESULTANT CARBON FIBERS

The process, structure, and property relationship of PAN fiber as a precursor to carbon fiber was studied. The limitations of stable spinning and property improvement associated with hot draw in solution spinning were found and quantified. Conditions were varied to generate precursor fiber up to the limit of draw, from which actual samples were collected for thermal conversion to carbon fiber. Samples of PAN and subsequent carbon fiber were characterized using tensile testing and x-ray analysis. The effects of draw on modulus and break stress, as well as the orientation of the crystalline structure of both parent precursor and resultant carbon fiber were found and related back to the quantified draw limit.

KEYWORDS: Draw, Solution Spinning, PAN fiber, Carbon Fiber, Hermans Orientation
Factor

Sarah Edrington

May 5, 2017

THE LIMITS & EFFECTS OF DRAW ON PROPERTIES AND MORPHOLOGY OF
PAN-BASED PRECURSOR AND THE RESULTANT CARBON FIBERS

By

Sarah Edrington

Dr. Rodney Andrews

Co-Director of Thesis

Dr. Matthew Weisenberger

Co-Director of Thesis

Dr. Haluk Karaca

Director of Graduate Studies

May 5, 2017

(For the girls)

ACKNOWLEDGEMENTS

The information, data, or work presented herein was funded in part by the Office of Energy Efficiency and Renewable Energy (EERE), U.S. Department of Energy, under Award Number:DE-EE0006926.

Disclaimer: The information, data, or work presented herein was funded in part by an agency of the United States Government. Neither the United States Government nor any agency thereof, nor any of their employees, makes any warranty, express or implied, or assumes any legal liability or responsibility for the accuracy, completeness, or usefulness of any information, apparatus, product, or process disclosed, or represents that its use would not infringe privately owned rights. Reference herein to any specific commercial product, process, or service by trade name, trademark, manufacturer, or otherwise does not necessarily constitute or imply its endorsement, recommendation, or favoring by the United States Government or any agency thereof. The views and opinions of authors expressed herein do not necessarily state or reflect those of the United States Government or any agency thereof.

I have many people to recognize for the love, support, help, and guidance I was given throughout this process. For the support from my friends and family. For your patience during long, late night, worry filled phone calls, thank you Mom.

I'd like to extend my thanks to my Carbon family at CAER. To John Craddock, David Eaton, and Ashley Morris, thank you for teaching me what it means to be a scientist and to Nik "Hoss" Hochstrasser and Jason Stewart, who helped make the chaotic process of solution spinning, a little easier.

I would lastly like to thank my advisor, Rodney Andrews and co-advisor Matt Weisenberger for their guidance and help in my studies, my research, and throughout this writing process.

TABLE OF CONTENTS

ACKNOWLEDGEMENTS..... iii

TABLE OF CONTENTSiv

LIST OF TABLESvi

LIST OF FIGURESvii

Chapter 1. Background 1

1 Introduction 1

1.2 Precursor Fiber Manufacturing 3

 1.2.1 Polymerization 4

 1.2.2 Solution Spinning 5

 1.2.3 Draw 6

 1.2.4 Limits of Draw 7

 1.2.5 The Deborah Number 7

1.3 Thermal Conversion to Carbon Fiber 8

 1.3.1 Stabilization 9

 1.3.2 Carbonization & Graphitization 9

1.4 PAN Precursor Fiber Characteristics 10

 1.4.1 Mechanical Properties 10

 1.4.2 Single Filament Tensile Testing 11

 1.4.3 Crystalline Structure 13

1.5 X-Ray Diffraction 14

Chapter 2. Investigation of Multi-Stage Hot Draw Limits 18

2 Introduction 18

2.1 Draw During Solution Spinning 18

 2.1.1 Experimental Methods 20

 2.1.2 Materials 24

 2.1.3 Solution Spinning 24

 2.1.4 Fiber Draw 25

2.2 Results 26

 2.2.1 Observations during spinning 27

 2.2.1.1 Visible Fiber Quality 27

 2.2.1.2 Line Tension Monitoring 28

 2.2.2 Microscopy 30

 2.2.3 Scale 32

2.3 Conclusion 33

Chapter 3. Mechanical Properties and Microstructure Approaching the Draw Limit	34
3 Introduction	34
3.1 Mechanical Properties	35
3.1.1 PAN Fibers.....	36
3.1.1.1 Tensile Testing	37
3.1.2 Carbon Fibers.....	38
3.1.2.1 Thermal Conversion to Carbon Fiber	39
3.1.2.2 Tensile Testing	39
3.1.3 System Compliance.....	40
3.1.4 Weibull Analysis.....	41
3.1.5 Results	42
3.2 Crystal Structure	49
3.2.1 X-Ray Diffraction Test Methods	49
3.2.2 Hermans Orientation	51
3.2.3 Scherrer Equation	52
3.2.4 Results	52
3.3 Conclusion.....	56
Chapter 4. Conclusion.....	58
4.1 Future Work	59
APPENDICES	61
Appendix A: Derivation of diameter/draw down ratio relationship	61
Appendix B: Single Filament Tensile Testing Data	62
Appendix C: Standard Operating Procedure for XRD Testing of PAN fiber	63
REFERENCES	76
VITA.....	79

LIST OF TABLES

Table 1.1 Comparison of the mechanical properties of typical aerospace materials [2].	1
Table 2.1 Sample DDR values along the line and the calculated DDR_{total} representation.	23
Table 2.2 Stable draw down ratios for first and second stage draw shown in figure 2.5 ..	29
Table 3.1 First and second stage DDR values for each fiber sample that was characterized in this study.	37
Table 3.2 The reported precursor values [31] and carbon fiber values obtained via Helium Pycnometry at UK CAER for bulk density were used by the Favimat+ to report diameter.	38
Table 3.3 Weibull modulus values for thermally converted PAN fibers for hot DDR_{total} obtained by linear regression of the equation for two-parameter Weibull distribution.	47
Table 3.4 Values for FWHM, crystal size (L_c), and Hermans orientation factor (f) for both PAN precursor and resultant carbon fibers for each DDR_{total} in hot draw during spinning.	54

LIST OF FIGURES

Figure 1.1 Schematic of a full scale wet jet solution spinning line at the University of Kentucky’s Center for Applied Energy Research [16]	5
Figure 1.2. Limits of draw or unattainable region of DDR represented by the theoretical Deborah number (De) [19].	8
Figure 1.3. General, simplified chemical mechanism showing the thermal conversion stages of PAN to carbon fiber [20].	9
Figure 1.4. Stress/strain curve of PAN precursor fiber obtained from single filament tensile testing.	12
Figure 1.5. Stress/strain curve of PAN based carbon fiber obtained from single filament tensile testing.	13
Figure 1.6. Molecular structure of a repeat unit of Polyacrylonitrile (PAN).	14
Figure 1.7. Helical packing of PAN chains as crystallization occurs.	15
Figure 1.8. Equatorial scan of PAN precursor fiber displaying (100) and (110) identifying crystal planes.	16
Figure 1.9. Equatorial scan of carbon fiber displaying (002) and (100) crystal planes.	16
Figure 2.1 Example Matrix of Experimental DDR Values.	21
Figure 2.2 ABB electric motor controlled roller used to guide fiber along the spinline, variations in roller speeds generate draw.	25
Figure 2.3 Graphic representing the DDR_{total} draw limit values (data labels) in terms of DDR_1 and DDR_2	26
Figure 2.4 “Fuzzy” fiber indicated by broken filaments resulting from high DDR_{total} values at the edge of the draw limit.	27
Figure 2.5 shows the recorded tensions at first and second stage draw plotted against hot DDR_{total} obtained in the investigation of the draw limit.	29
Figure 2.6 Cross sectional 2k mag view of fiber right out of coagulation pre-hot first and second stage draw.	30
Figure 2.7 Fiber post hot first and second stage $DDR_{total}=3.18$ draw at 2k high mag (left) 8k high mag (right).	30
Figure 2.8 Side view SEM images of PAN (i) fiber out of coagulation, pre-hot draw (ii) precursor fiber post hot $DDR_{total}=3.18$ (iii) Carbonized fiber post hot $DDR_{total}=3.18$	32
Figure 3.1 Visual representation of (a) 500 filament count fiber tow, (b) Individual filament fibril microstructure.	34
Figure 3.2. Plot of average PAN precursor fiber break stress vs. DDR_{total} of ($N > 75$).....	43
Figure 3.3 Plot of average resultant carbon fiber break stress vs. DDR_{total} ($N \geq 40$).....	44
Figure 3.4. Plot of average PAN precursor modulus vs. hot draw DDR_{total} ($N > 75$).....	45
Figure 3.5 Plot of resultant carbon fiber corrected modulus vs. hot draw DDR_{total}	46
Figure 3.6 Distribution of failure probability vs. tensile stress using Weibull analysis ($N \geq 40$) for resultant carbon fiber.	47
Figure 3.7. Weighted effects of first and second stage draw on the mechanical testing results. (From top left to bottom right, PAN modulus, PAN break stress, carbon fiber modulus, carbon fiber break stress.)	48
Figure 3.8 Schematic of the rotations in X-ray analysis of fiber.	50

Figure 3.9. Azimuthal scans at (100) plane of PAN precursor fiber spin and gel drawn at DDR= 1.52, (b) combined spin, gel, and hot drawn at DDR=1.52 x 3.18=4.83, (c) after thermal conversion to carbon fiber.	53
Figure 3.10 Calculated Hermans Orientation Factors for PAN precursor fiber vs. DDR_{total}	55
Figure 3.11 Calculated Hermans Orientation Factors for resultant carbon fiber vs. DDR_{total}	56

Chapter 1. Background

1 Introduction

Current materials research and development is highly focused on the creation of lightweight, strong materials to improve performance and efficiency of modern day technologies. An example is the use of lightweight composite materials as a replacement for steel and aluminum in high performance applications. Composite materials are a combination of two or more materials possessing complementary mechanical, thermal, or chemical properties.

Composite materials play a large role in the aerospace and automotive industries, driven by the ever-growing need to reduce weight and improve efficiency while meeting emission and safety standards [1]. However, the use of these materials has been limited due to the high cost associated with manufacturing of raw materials in comparison to the current materials, aluminum and steel. For widespread application of these materials, manufacturing cost of raw materials is an obstacle that must be overcome.

One of the most popular composite materials used in these industries is Carbon Fiber Reinforced Composite (CFRC), composed of high modulus and strength to weight ratio carbon fiber reinforcements and a matrix material. The carbon fibers supply the mechanical properties possessing much higher modulus and strength values per density than aluminum and steel. A comparison of the modulus and strength per density of typical aerospace grade aluminum alloy, steel, and carbon fiber is shown in Table 1.1.

Table 1.1 Comparison of the mechanical properties of typical aerospace materials [2].

	Tensile Strength (MPa)	Modulus (GPa)	Density (g/cm³)	Modulus/ Density	Tensile Strength/ Density
IM7 Carbon Fiber	5516	276	1.78	155	3099
Aluminum 2024-T3	483	73	2.78	26	174
AISI 4130 Steel	670	205	7.85	26	85

Its excellent properties and versatilities make optimization, quality control, R&D, and most of all cost reduction, the focus of today's carbon fiber manufacturing industry. A specific area of interest in industry is the improvement of carbon fibers at their foundation with precursor or starting material selection.

1.1 History

Carbon fibers have been present since the gathering of cotton as a source of fabric, as these cellulosic fibers were exposed to heat, unknowingly pyrolyzed into carbon fibers [3]. The carbonization process of cotton filaments was again observed in Edison's work with the development of the incandescent lightbulb [4]. In the early instances of the discovery of this material, cotton precursor was accidentally thermally converted to carbon fiber. Since then, precursor materials have improved and more sophisticated materials have been developed, increasing the popularity of carbon fiber.

In the 1950s textile industry, synthetic cellulosic rayon was popular and eventually used as the first precursor fiber for large-scale carbon fiber manufacturing. Rayon was used as the only precursor for carbon fiber by the space program because of its low thermal conductivity and porous structure, but manufacture was phased out in the U.S. due to environmental and health impacts of viscose rayon manufacturing [5]. The need for an equal or better performing material was high for the continuation of space and aerospace travel as well as the growing interest in light-weight, high-efficiency travel.

The replacement for rayon as a carbon fiber precursor was polyacrylonitrile (PAN), a synthetic, acrylic fiber, known for its mechanical properties and high-carbon yield. PAN remains the most popular precursor material for carbon fiber manufacture because of the relatively low cost and high-carbon yield after thermal conversion. The carbon fibers that result from this material also possess high strength and modulus values. The use of PAN-based carbon fibers for high-strength applications is still growing in popularity today. In recent years, use has begun to move away from very narrow, expensive military and space applications to larger scale manufacturing industries like the automobile industry. In the automobile industry, a wider market, manufacturing cost savings is essential to grow and remain competitive.

The Boeing company, one of the largest consumers of carbon fibers, introduced the 787 Dreamliner in 2011 with an airframe comprised of 50 wt% composites, largely CFRC materials. Accompanied by a 20 percent reduction of fuel burn and emissions, this was the largest use of composite materials in commercial aerospace yet [6]. Mainstream market automotive companies are beginning to implement carbon fiber composites into body components to reduce weight and meet fuel emissions standards. This movement has been slow due to the high cost of raw materials and manufacturing processes of the carbon fiber reinforcements. In comparison to steel and aluminum materials currently used in automobiles, carbon fiber composites cost roughly 20 times more to manufacture [7]. These high costs are the result of the carefully controlled process of precursor fiber spinning and multistep high temperature conversion to carbon fiber. To make carbon fiber composites a reality in mainstream technologies, manufacturing costs would ideally be reduced to \$5 per pound from the current \$15 per pound [8]. PAN is the preferred precursor material for carbon fiber manufacturing due to the low cost of raw materials and ease of processing, however more work must be done to make these processes affordable for industrial use of PAN-based CFRC.

1.2 Precursor Fiber Manufacturing

Radical polymerization of acrylonitrile, solvent/polymer dissolution, fiber formation via solution spinning, fiber draw, and thermal conversion by stabilization and carbonization [4] are required in the multi-step conversion of raw PAN polymer to carbon fiber. Carbon fibers can be created by several conversion processes from a variety of precursor materials. However, precursor material selection lays the ground for carbon fiber properties and performance. Resultant carbon fiber properties depend greatly on the processing conditions and properties developed during precursor manufacturing [9]. Commonly used industrial carbon fiber precursors include PAN, cellulose, and pitch-based materials, depending on the application [4]. PAN based carbon fibers dominate the current carbon fiber market, consisting of 90 percent of the market share [10].

The precursor fiber formation or “spinning” processes are of great interest in materials research and industry. Some fiber forming techniques are electrospinning, melt spinning,

dry spinning, dry jet (solution) spinning, and wet jet (solution) spinning. Electrospinning however, is a very difficult-to-scale process of combining discontinuous fibers of varying sizes or additives to the fiber [11] and therefore not suitable for high strength continuous carbon fiber precursor manufacture.

The simplest continuous spinning process is melt spinning. Melt spinning is conducted by extruding the polymer through a die-head spinnerette above the melting temperature of the polymer, followed by fiber solidification after exposure to the lower temperature air. Due to the degradation of PAN at temperatures below its melt temperature, melt spinning is generally not a suitable spinning technique [12].

In wet jet solution and dry jet solution spinning, a polymer/solvent mixture is extruded through a spinnerette into a coagulation bath containing a mixture of solvent and nonsolvent resulting in a dual diffusion process. During this diffusion process, solvent exchange occurs to remove the solvent from the polymer and nascent polymer filaments begin to take shape. The difference between wet jet and dry jet solution spinning is the presence of an air gap before coagulation in dry jet spinning [12]. Successful wet jet and dry jet solution spinning requires a careful multivariable balance that can be difficult to optimize and obtain, but once determined can be very beneficial in the processing and customization of acrylic fibers. Each precursor material has a spinning process best suited to the materials behavior and therefore all methods may not be appropriate. Given the readily soluble composition of the polymer, continuous PAN fibers are most commonly processed in industry at large scale using wet jet solution spinning.

1.2.1 Polymerization

PAN polymerization is initiated using free radical polymerization of acrylonitrile and a comonomer, most frequently methyl acrylate or methyl methacrylate and an organic acid (methacrylic or itaconic acid) as a catalyst for thermal conversion [13]. Pure homopolymer PAN is difficult to dissolve, and is not widely used in the fiber spinning industry [12]. Copolymers are used to blend polymer properties, to improve solubility, and improve processability [14] by lowering glass transition temperature, changing reactivity, and controlling oxidation temperature [15]. PAN can be polymerized using solution, emulsion,

bulk, and suspension polymerization techniques, depending on the scale and method of spinning.

1.2.2 Solution Spinning

The most common method of obtaining high quality PAN fibers at industrial scale is wet jet solution spinning. More complex than melt spinning techniques, solution spinning requires the coordination of many spinning parameters such as solvent/non-solvent composition, temperatures, draw ratios, and line speeds. Accompanying the difficulty of obtaining a well-balanced group of parameters is the ability to optimize and customize fiber characteristics such as diameter, cross sectional shape, surface area, porosity, and microstructure, to produce high quality carbon fibers for application in CFRC.

The spinning process begins with the preparation of a polymer dope (or spinning solution) by mixing PAN polymer with solvent at an increased temperature for several hours to allow for polymer dissolution. The polymer dope must then be degassed under vacuum to remove any gas from the mixture and ensure continuity in the flow. Even tiny bubbles lead to defects with spinning filaments with diameters on the order of 10 microns. A fully mixed and degassed dope is then ready for solution spinning. Figure 1.1 shows a schematic of a solution spin line as the dope, traveling from left to right, is spun into PAN precursor fiber.

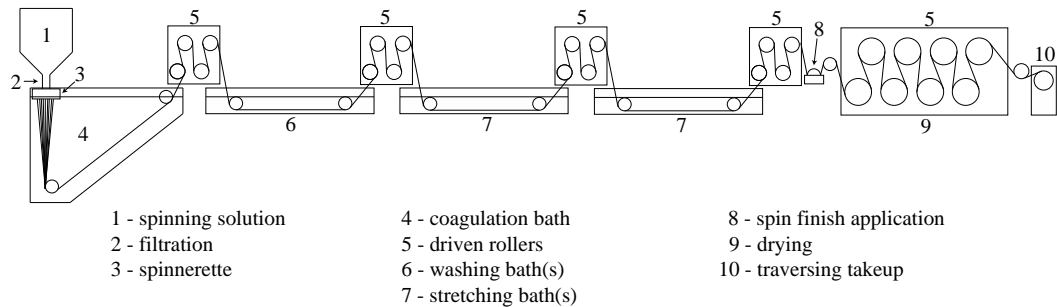


Figure 1.1 Schematic of a full scale wet jet solution spinning line at the University of Kentucky's Center for Applied Energy Research [16].

Using a high precision pump, dope is metered through a filter and diffuser system to ensure pressure uniformity and debris removal (1-2 in figure). Filtered dope is then extruded through a spinnerette with capillaries 10s of micron in diameter, directly into a temperature and concentration-controlled solution where coagulation occurs (3-4 in figure). The solvent exchange in coagulation is largely immediate and results in the solidification of fibers, development of the fibril structure, and the formation of pores caused by the solvent transfer from the polymer to the coagulation bath. Fibers are pulled from the spinnerette, through the coagulation bath and into a more dilute solution bath by driven rollers which control the speed of the line (5). From here, fiber is subjected to additional wash (6) followed by heated water and glycerol baths for stretching (7). The fiber is washed in hot water again for removal of heat transfer draw medium, glycerol, spin finish is applied, fiber is dried, and collected on a traversing collection spool (8-10).

1.2.3 Draw

One of the most important steps in solution spinning and the formation of PAN fibers is the stretching process, also referred to as “draw.” Draw is essential to nascent fiber and microstructure formation of the fibrils, the foundation of PAN precursor properties that are carried through to carbon fiber properties.

Draw occurs in multiple steps throughout the process: at extrusion as spin draw in the coagulation bath, as gel draw in the second bath, and at an increased temperature in spin draw as hot draw. At the relatively low speeds and solvent exchange in solution spinning, there is very little orientation that occurs due to draw in coagulation in comparison to melt spinning. An additional two-step hot draw is therefore necessary to promote alignment in the polymer chains with the fiber axis [14].

Hot draw in fiber spinning is performed in a hot liquid or steam chest to change the fiber length and cross sectional area. Above T_g , the polymer chains are in the rubber state where free volume is high and molecules have more energy and space to move and change conformation [17] under axially applied tension, resulting in lengthening of the fiber.

Complying with the conservation of mass, as the fiber lengthens, the fiber structure also begins to change as the diameter shrinks, pores formed in coagulation begin to collapse,

and the fiber densifies. The fibrils that make up the ligaments in the porous structure are pulled in the direction of draw to align with the axis of the fiber.

As the nano-sized fibrils align, so do the molecules that make up the structure of semi-crystalline PAN, composed of crystalline and amorphous regions. As these chains align, the crystal and amorphous regions align and their properties are reflected on the fiber in the direction of orientation.

1.2.4 Limits of Draw

Draw in fiber spinning is necessary for the improvement of mechanical properties. Draw increases orientation with the fiber axis and thus improves the modulus (E) in this direction. The mechanism of draw also decreases diameter and densifies the material as pores in the structure begin to collapse. This densification reduces the probability of defects and improves the break stress, which is largely dependent of the number of defects per unit length. However, there are limits to this mechanism that have not been widely studied and defined. At the tow level, the result of reaching the limits of draw is the accumulation of filament breakage as the cross sectional area decreases to a point that cannot support the applied load [18]. Understanding and quantifying the draw limit will prevent breaks in the line and improve fiber quality and performance. Precursor fiber properties are generally directly translated to carbon fiber properties. Precursor that is easy to handle with a uniform tow is essential to create a carbonized material of the same quality. Carbonizing a precursor fiber with poor qualities and broken filaments will result in poor quality carbon fiber and additional filament breakage through the thermal conversion process.

1.2.5 The Deborah Number

A dimensionless variable, the Deborah number (De) is used to describe the flow behavior when stretching liquids of varying viscoelastic properties. This value can be used to find the behaviors of a material during draw and as shown in figure 1.2, an unattainable zone in relation to drawing of a polymer, or a theoretical limit to draw.

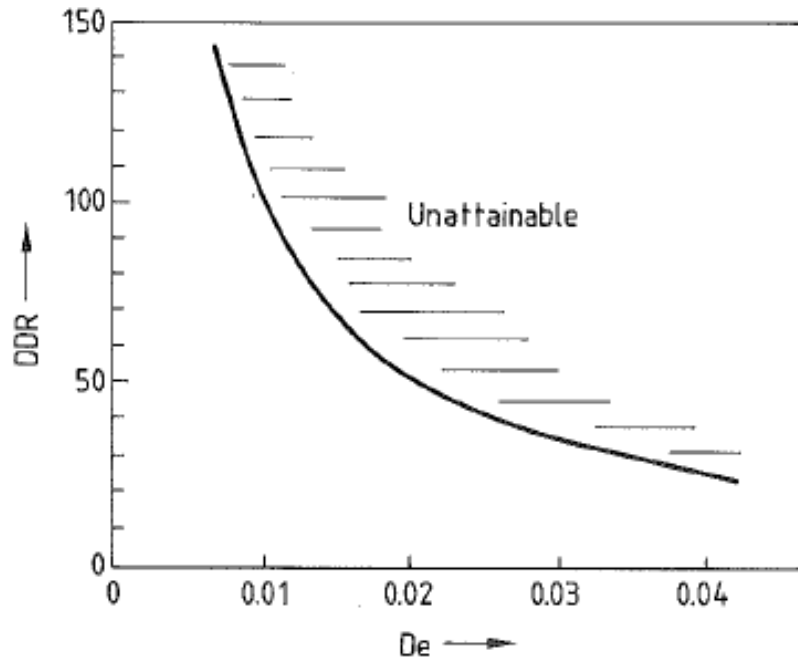


Figure 1.2. Limits of draw or unattainable region of DDR represented by the theoretical Deborah number (De) [19].

1.3 Thermal Conversion to Carbon Fiber

To acquire the desired material properties of a strong, lightweight material, PAN-based precursor fibers must be thermally converted to carbon fiber. During this process, precursor fiber goes through significant physical and chemical changes to be converted to carbon fiber. This multi-step process includes stabilization, carbonization, and sometimes graphitization. Each step of thermal conversion requires a careful temperature and time profile to allow linear PAN polymer chains to cyclize and crosslink to the ordered structure of carbon fiber [12]. Figure 1.3 shows the changes of the chemical structure of PAN throughout the thermal conversion process to carbon fiber.

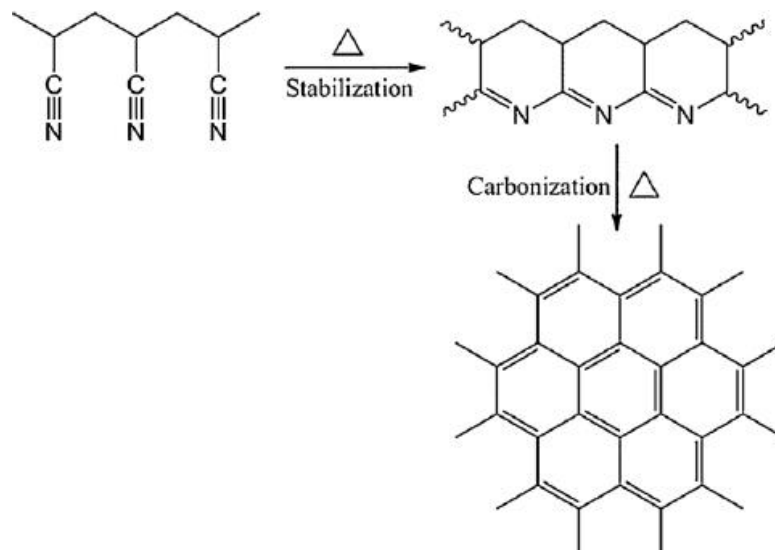


Figure 1.3. General, simplified chemical mechanism showing the thermal conversion stages of PAN to carbon fiber [20].

1.3.1 Stabilization

Thermal conversion begins with oxidative stabilization, during which pendant nitrile groups are cyclized [14] pictured in figure 1.3. This conversion is usually done under temperatures in the range of 200-250°C for a predetermined time depending on the fiber characteristics [4]. The molecular structure of PAN is altered in this state as the fiber in an O₂/N₂ atmosphere is heated, the polymer chains are joined in a ladder formation, prepping the structure for the changes to come in carbonization [4]. The structure of PAN is fully amorphous at the end of this step [21]. Stabilized PAN precursor fibers are not fully converted to carbon fiber, containing only 60-70 percent carbon [9], to create a more perfect carbon structure further heat treatment is performed. The stabilization process renders the PAN as ladder polymer, partially cross-linked by oxygen, and infusible upon heat treatment to carbonization temperatures.

1.3.2 Carbonization & Graphitization

Differing from stabilization, carbonization is performed at higher temperatures, for longer periods of time, and in an inert gas environment, generally helium (He), with the fibers under tension. Most remaining non-carbon elements of the stabilized fiber are eliminated

as volatiles, resulting in a mass loss nearing 50 percent [14]. Ladder polymer fuses and begins to form graphitic structure comprising carbon fibers [12] and a mostly crystalline structure remains. The density of the material increases with heat treatment as the molecular weight of the components increases and a highly ordered graphitic structure is formed [22]. Temperatures can reach well above 1000°C, varying with respect to precursor fiber and anticipated carbon fiber properties. This step brings the material to over 90 wt% carbon [4].

When producing carbon fibers with very high modulus, an additional step of graphitization is necessary. At temperatures above 2000°C, the graphitic structure becomes more ordered and annealed, and orientation improves, thus improving the fiber modulus [14]. The carbon content increases to over 99 wt% to an almost pure carbon structure [4].

1.4 PAN Precursor Fiber Characteristics

PAN is the dominant precursor material because of its high carbon content and capacity to generate both high modulus and high toughness (high strain to failure, high strength) carbon fibers. Quantification of mechanical properties can provide insight into the performance of the carbon fibers to be used to optimize and customize material performance.

1.4.1 Mechanical Properties

The forces between oriented repeat units provide strength and stiffness in the PAN polymer chains and as the crystals align, their anisotropic nature is carried through to the properties of the fiber itself [17] and fiber modulus improves. However, the tensile strength of the fiber is not wholly dependent on this alignment. Instead, defects and voids present in the material govern strength.

The irregular, atactic PAN stereochemistry does not allow for complete crystallization and perfect packing in the structure. As a result, regions where the packing is less dense due to the irregularity of the structure result and form defects, reducing the maximum tensile stress [3].

The connection between crystalline orientation and mechanical properties is well known in materials processing and has been used in many studies to customize the properties of polymer fiber for a desired application. Song et. al used this connection to improve mechanical properties of electrospun PAN fiber in nanocomposites by hot-stretching [11] and Newcomb et. al studied draw in gel spun PAN fiber orientation to improve strength [23]. The many studies of the processing/properties/structure of PAN have provided the understanding of their relationship and a way to calculate the theoretical limits of draw. However, experiments to determine actual draw limits have not been widely conducted and studied. Understanding the effects of the processing limits on the mechanical performance will optimize the spinning process and customization of the product for a wider use at a lower cost.

1.4.2 Single Filament Tensile Testing

The mechanical performance of PAN fiber is quantified by Young's modulus of elasticity (E) and break stress (σ) (tensile strength). The values for these properties can be determined from the stress and strain measurements obtained when fibers are subjected to tensile forces. The test method often used to obtain these measurements is single filament tensile testing.

Length changes (Δl) with respect to initial gauge length (l_i) and axial forces (F) measured by a load cell are collected by a tensile test instrument and used to calculate stress (σ) and strain (ϵ) on the filament using the fundamental equations for stress and engineering strain of a cylindrical rod of cross sectional area (A) (eq 1.1, 1.2).

$$\sigma = \frac{F}{A} \quad [1.1]$$

$$\epsilon = \frac{\Delta l}{l_i} \quad [1.2]$$

Data is collected from sample failure and used to determine the limits of performance. The Favimat+ Single Filament Tensile Testing System is an instrument developed for the textile

industry to test individual filaments for axial mechanical properties. The instrument applies an axial force on the samples in the form of a crosshead clamp moving one end at a constant speed until failure. Both plastic and elastic response in the stress/strain curve of PAN fiber is shown in figure 1.4.

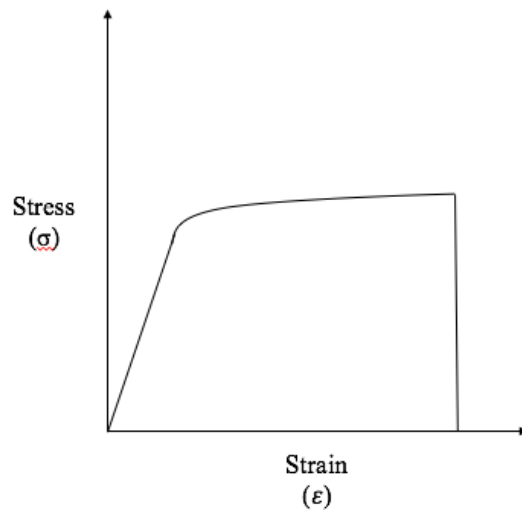


Figure 1.4. Stress/strain curve of PAN precursor fiber obtained from single filament tensile testing.

The material elastically deforms first as the amorphous regions elongate allowing crystalline regions to align. Once fully aligned, plastic flow occurs in the amorphous regions and covalent bonds in the crystalline structure can begin to break resulting in further plastic deformation and eventually failure by necking [17].

During conversion to carbon fiber, the nitrile group is removed, the polymer chains become cross-linked, and the percent crystallinity of the material increases [14]. This molecular change is shown in the brittle, elastic nature of carbon fiber and the stress/strain curve in figure 1.5., as the fiber's plasticity is lost.

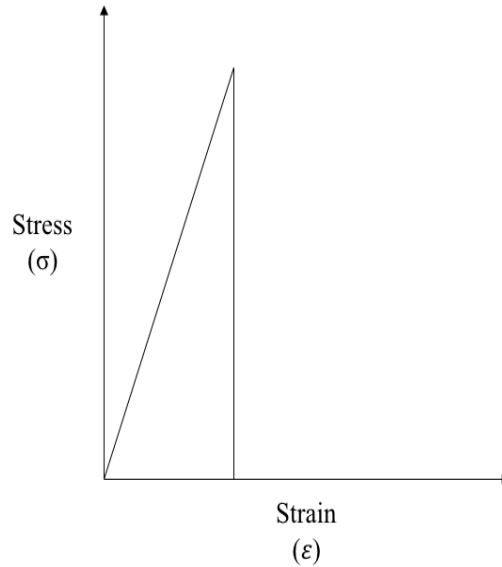


Figure 1.5. Stress/strain curve of PAN based carbon fiber obtained from single filament tensile testing.

From the stress/strain curves of PAN precursor and carbon fibers, break stress is identified as the stress corresponding to a sudden drop in stress due to material rupture. Young's modulus of elasticity is defined in equation 1.3 as the slope of the stress/strain curve. PAN precursor fiber modulus is defined only by the initial modulus, before plastic deformation occurs, while carbon fiber modulus is defined by the single region of linear elastic deformation. Carbon fiber stress/strain curves are expected to display a steeper stress/strain slope than PAN precursor fiber because of the increase in modulus.

$E = \frac{\sigma}{\epsilon}$	[1.3]
-------------------------------	-------

Calculations made by the Favimat instrument for stress, strain, and modulus can then be used to determine the fiber strength and relative stiffness.

1.4.3 Crystalline Structure

Features of the molecular structure of PAN fibers are very influential in the development of the mechanical properties of the filaments. PAN polymer chains are composed of repeat

units of acrylonitrile that form a carbon backbone with bulky nitrile side group as shown in Figure 1.6.

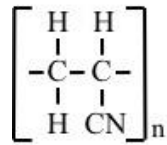


Figure 1.6. Molecular structure of a repeat unit of Polyacrylonitrile (PAN).

The relatively flexible and repetitive structure of these chains containing small nitrile functional groups with atactic isochemistry allow only for semi-crystallinity at a maximum of 50 percent [12]. The dense packing needed for crystallization is more difficult and the polymer must take an isotactic or syndiotactic configuration to begin to crystallize [17]. The semi-crystallinity creates a structure of varying crystal and amorphous regions as dense packing is not possible where the bulky side groups are randomly present. The amorphous regions have low modulus in a rubbery state, while the crystals possess high modulus in a more rigid state [18].

Crystals typically form in polymer chains by the controlled cooling from the melt temperature where chains move more freely, to the glass transition temperature where the chains are essentially frozen [17]. However in fiber spinning, line speeds also contribute to this process as stress can also induce the nucleation of crystals [14]. In addition to crystal formation, percent crystallinity, crystal size, and orientation of the crystals also increases with hot fiber draw in PAN spinning [11] altering the atomic structure significantly. Thermal conversion to carbon fiber also changes the crystal structure of the material. In the stabilization step, almost all crystalline structure is removed, leaving an amorphous structure. Recrystallization then occurs in carbonization, resulting in increased performance of the final material [21].

1.5 X-Ray Diffraction

For high performance applications, the atomic structure of the crystals is of great interest. Studies show that the orientation of the crystal structure of PAN fiber is the source of the high modulus that PAN fibers must possess to be converted to high performance carbon

fibers [24]. Crystallinity, crystal size, and orientation quantified by Hermans orientation factor (f) are used to characterize the atomic structure of the fiber and can be determined using X-Ray Diffraction techniques [9, 11, 14, 25].

The chains take a helical arrangement to allow for tight packing of the irregular nitrile functional group, stacking these hexagonal configurations, as shown in Figure 1.7. to form the crystalline regions of PAN. The organization of this packing can reveal a lot about the properties of the macromolecular chains as well as the properties of the resulting fibers. From the repetitive nature of a polymer, patterns can be identified as the unit cell of the structure. A single unit cell can contain many repeat structures.



Figure 1.7. Helical packing of PAN chains as crystallization occurs.

Using x-ray diffraction (XRD), much can be learned about the polymer structure and composition. In this technique, x-rays are focused and diffracted from a sample, and the intensities and angles of the diffraction pattern are then used to identify and characterize the substance. Crystal plane spacing in a crystal structure is unique to every substance, making it a useful aid in identifying the composition of a substance [26]. The molecular composition can be determined and used to identify an unknown substance by comparison against known elemental diffraction patterns. Angles (θ) associated to peaks in a diffraction pattern are used to identify crystal plane spacing (d) using Bragg's law (eq 1.4) for a wavelength (λ) and intensity (n).

$$n\lambda = 2d_{hkl} \sin \theta \quad [1.4]$$

The diffraction pattern of an equatorial scan of PAN fiber and carbon fiber can be seen in Figures 1.8. and 1.9. The PAN fiber peaks at $2\theta=16.6^\circ$ and 29.5° represent the Bragg angles associated with the (100) and (110) planes. These planes correspond to a nearly perfect hexagonal spacing of 6.0 \AA [27] represented by the lattice parameters $a=c=6.17 \text{ \AA}$ [28], which define the unit cell dimensions.

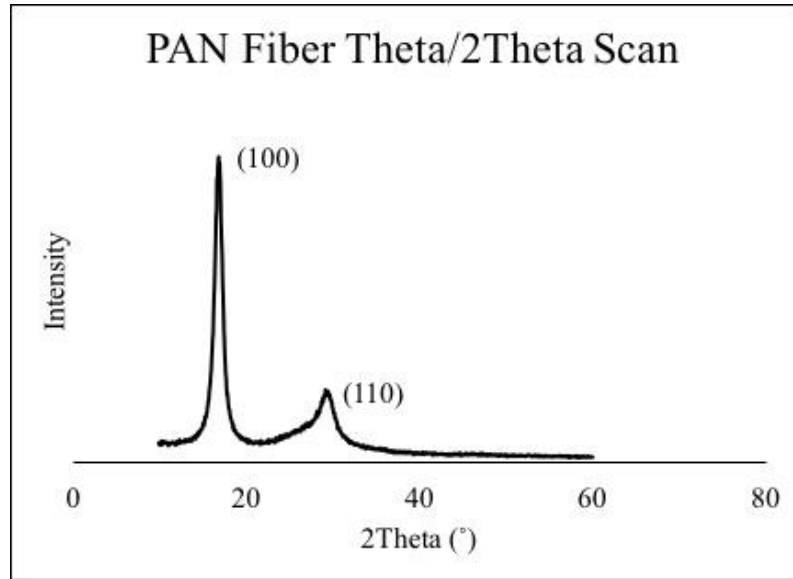


Figure 1.8. Equatorial scan of PAN precursor fiber displaying (100) and (110) identifying crystal planes.

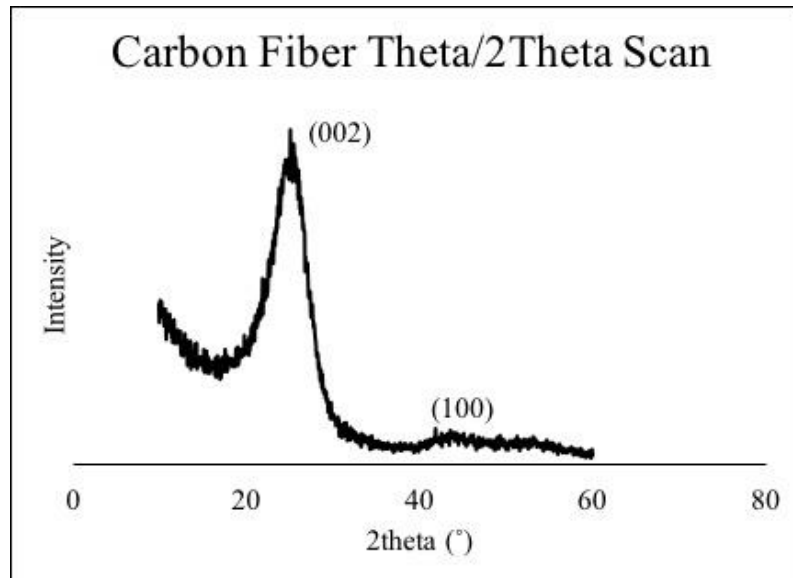


Figure 1.9. Equatorial scan of carbon fiber displaying (002) and (100) crystal planes.

In the conversion to carbon fiber, PAN fiber is subjected to a series of heat treatments in which the crystalline structure and fiber properties change significantly. Zhu et. Al reported that after stabilization, the fiber loses almost all crystalline structure of PAN and recrystallizes some in carbonization, never to return to the high crystallinity present in PAN precursor fibers [21], the same can be said for the orientation. The resulting crystal structure of carbon fiber is shown by the peaks at Bragg angles $2\theta = 25^\circ$ and 42° representing the (002) and (100) planes in figure 1.9.

Each peak in the equatorial scan (figure 1.8. and 1.9.) represents an elemental crystal unit cell and can be further investigated for structure and alignment about any axis of interest. As previously mentioned, PAN fiber crystals are anisotropic as they usually lie in the processing direction of the fiber axis. The anisotropic nature of these fibers leaves directions perpendicular to the axis very weak and the direction of high strength, modulus of interest along the axis of the fiber.

In PAN fiber, the crystalline properties of interest are the percent crystallinity and the orientation the crystals in the direction of the fiber axis. A highly crystalline structure in the direction of the anticipated tensile stresses will result in a stiffer and stronger fiber. Therefore, an additional investigation of the Bragg angle corresponding to a crystal plane is performed using an azimuthal scan about the meridian axis, from which the peak shape and intensity is used to determine crystallinity and orientation of the fiber with the axis of interest [9].

In this study, the limits of two-stage hot draw during precursor spinning will be studied and quantified by systematic DDR variation experiments. Determining the DDR conditions that result in unstable processing will allow for better control of complex fiber spinning, and quantitative definition of the limit of draw. Additionally, precursor will be converted to carbon fiber, both sample sets will be tested, and their mechanical properties and microstructures will be compared. This work seeks to uniquely correlate the precursor drawing process to the mechanical properties and microstructures of both the precursor and resultant carbon fiber.

Chapter 2. Investigation of Multi-Stage Hot Draw Limits

2 Introduction

Polyacrylonitrile (PAN) polymer fiber, the dominant precursor material used for the manufacture of high performance carbon fiber can be produced using one of two fiber spinning techniques: dry spinning and wet spinning. PAN begins to degrade below the melting temperature (300°C) required for processing and therefore cannot be manufactured using simple melt spinning. In wet spinning, also known as solution spinning, a coagulation step allows for valuable fiber manipulation as the structural fibrils form via solution exchange from the extruded fiber into a coagulation solution bath. As this exchange occurs, extension by acceleration promotes alignment of the fibrils in the direction of draw and thus orientation of crystalline structure from which they are made. This increase in alignment of fibrils with the axis of the fiber tow will result in moduli improvement, for this reason wet spinning is the preferred method of fiber formation in industry [12]. In addition to the alignment occurring during fiber formation in wet spinning, PAN crystalline structure aligns more perfectly with the axis and fibrils densify further down the line in additional draw zones using line acceleration and elevated temperatures. The atomic and macrostructure changes experienced by the fiber in solution spinning have a great impact on the resultant properties of precursor to be converted to carbon fiber.

2.1 Draw During Solution Spinning

The most impactful spinning parameter on the elastic modulus of PAN fiber is stretch or “draw,” which is responsible for the formation of the final geometry and morphology of the fiber. Draw not only influences the geometry and morphology of the fibers, but also the properties necessary to be used as a carbon fiber precursor material [24]. At UK CAER, draw is applied to fiber in three regions during solution spinning; spin draw, gel draw, and in combined first and second stage hot draw. First is spin draw, where nascent fibers are formed through the coagulation process. This is where the newly formed fibril structure begins to align and the foundation of the fiber is born. Gel draw follows, where coagulated

fiber, still in a solvent-plasticized state, is drawn through an additional bath containing 50 wt.% solvent. To eliminate any residual solvent from the fiber, the fiber is pulled through water wash baths and then first and second stage hot draw is conducted near and above the glass transition temperature. After this, the fiber is washed to remove surface draw medium from the second stage draw process.

Entering first and second stage hot draw, the fiber has been washed of solvent, no additional solvent exchange occurs, and pore formation is complete. This step manipulates and collapses these pores, densifies the material, and aligns the fibrils and the molecular crystal regions of this structure more perfectly with the axis. Most of the mechanical property formation of the final product occurs here and is highly dependent on the fiber structure and any void content.

To manipulate the fiber in this state, an increase in temperature is needed to relax the polymer chains and thus promote movement in the direction of draw and increase orientation [17]. Hot draw is done in both steam and hot liquid mediums, which transfer heat quickly to allow for sufficient draw at high speeds and high draw. Industry primarily uses a steam stretching approach. This study, however, utilized a two-stage hot liquid draw system and focuses on the draw relationship of first and second stage hot draw. Spin draw and gel draw are important parameters in fiber formation but will not be discussed.

The parameter of draw can be quantified by the Draw Down Ratio (DDR) and is defined in equation 2.1 as the ratio of the linear speed of the fiber exiting draw (v_1) to the linear speed of the fiber entering draw (v_0).

$$DDR = \frac{v_1}{v_0} \quad [2.1]$$

The mechanism of draw and the associated geometry change can be explained by the conservation of mass as the resulting axial lengthening of the fiber is accompanied with an equivalent decrease of fiber diameter and densification as pores collapse. There are obvious limits to this draw mechanism and as the fiber lengthens, the shrinking diameter will eventually be unable to support the load of the tensile force, resulting in filament breakage. However, it is widely known in the fiber industry that an increase in fiber draw will result in better mechanical performance [29]. It is therefore the interest of this study to find the

limits to first and second stage hot draw that produce high strength fiber while maintaining a stable, continuous spinning process. The following explains the experimental methods used in defining the draw limits for DDRs at first and second stage hot draw in PAN fiber solution spinning. The following methods are intended to provide an experimental procedure to methodically determine the limits of draw in any solution spinning setting equipped with two-stage hot draw. It is important to note that the results of these experimental methods will vary with deviation from the many variables associated with this experimental solution spinline and are specific to the viscoelastic properties of this polymer fiber spinning process.

2.1.1 Experimental Methods

The draw limit for first and second stage hot DDR values was found over a series of experiments designed to result in a complete break of the fiber tow and unstable spinning conditions. All spinning process parameters such as temperature, flow rate, and solvent concentrations remained constant, except for first and second stage hot DDR. Experimental parameter combinations in the form of first and second stage draw (DDR_1 and DDR_2) were organized in matrix form as shown in figure 2.1. The experimental organization was inspired by the Deborah number theoretical unattainable region of DDR discussed previously.

draw limit. Microscopy of the fiber before and after hot draw cross sections and surface morphology was also conducted.

DDR is a multiplicative variable. The total draw along a spinline, is obtained by the product of all DDR values in the process. This includes spin draw, gel draw, first and second stage draw, any draw in wash baths, and at take-up. Equation 2.2 shows the simple relationship between each DDR and the total draw on the fiber.

$$DDR = DDR_{spin} \times DDR_{gel} \times DDR_{1st} \times DDR_{2nd} \dots \times \dots DDR_{n-1th} \times DDR_{nth} \quad [2.2]$$

$$DDR = .76 \times 2.09 \times 1 \times 1 \times 1 \times 1 \times DDR_1 \times DDR_2 \times 1 \times 1 \times .98 \quad [2.3]$$

$$DDR = (1.56) \times (DDR_1 \times DDR_2) \quad [2.4]$$

Table 2.1 Sample DDR values along the line and the calculated DDR_{total} representation.

Sample DDR values		
Roller	Linear Speed (m/min)	DDR
Spinnerette	1.2026	
DDR_{spin} Constant		0.76
y_0	0.91	
DDR_{gel} Constant		2.09
y_1	1.9	
Wash Constant		1
y_2	1.9	
Wash Constant		1
y_3	1.9	
Wash Constant		1
y_4	1.9	
Wash Constant		1
y_5	1.9	
First Stage Hot Draw (DDR_1)		1.95
y_6	3.71	
Second Stage Hot Draw (DDR_2)		1.7
y_8	6.3	
Wash Constant		1
y_9	6.3	
Wash Constant		1
Heated Roller	6.32	
Take-up draw Constant		0.98
Take-Up	6.17	
DDR		5.16

The calculation in equation 2.3 shows a sample DDR calculation for total draw in a typical solution spin run using conditions in table 2.1. This calculation includes spin and gel draw as well as hot draw and take-up draw. It should be noted here that the spin draw < 1 due to the complexity in the many variables involved at coagulation the material shrinks and swells, resulting in DDR values often less than one [30].

For these series of experiments, spin draw, gel draw, and draw in wash baths remained constant to focus on the effects of first and second stage hot draw. Therefore, the combinations of first and second stage hot draw DDR that comprise the draw limit will be represented and compared to one another as $DDR_1 \times DDR_2 = DDR_{total}$ neglecting the constant draw from spin and gel draw. Using equation 2.3, the resulting DDR_{total} value for

only the variables of interest, *first and second stage hot draw* (DDR_1 and DDR_2), can be calculated.

2.1.2 Materials

These experiments were performed using UK CAER's polymer fiber solution spinning line. The polymer solution was composed of a 300,000 M_w , 13.5 wt% polyacrylonitrile (PAN) (2 mol% co-methyl acrylate, 1 mol% co-methacrylic acid) in N,N-Dimethylacetamide (DMAc). The solids content of the mixture used for this study was determined previously to obtain baseline precursor fibers with circular cross sections and good surface morphology.

2.1.3 Solution Spinning

A 500 ml batch of 13.5 wt% PAN in DMAc mixture was prepared and allowed to mix overnight in a cylindrical mixing vessel, complete with a heating jacket to ensure proper temperature control. Temperature ramps went to 50°C to allow polymer dissolution under uniform mixing. Once mixing was completed, the dope was extracted into a Teledyne ISCO 500D, high-precision, high-pressure syringe pump, where it was degassed under vacuum overnight. Once fully mixed and degassed, the dope was ready for the spinning process.

Dope was filtered through a 50°C heated manifold of five 7 micron filters in parallel, followed by a series of plates to apply uniform pressure across the spin head. Once evenly distributed, the dope was filtered through a final mesh filter before extruded through a 500 hole, stainless steel spinnerette (hole diameter = 60 micron) at a start-up flow rate of 3 ml/min. The coagulation bath consisted of 77.5 wt% DMAc/H₂O and was temperature controlled at 17°C. After coagulated fiber was pulled to the first roller, the flow rate was stepped down to the desired rate of 1.7 ml/min in 0.2 ml/min increments. At this flow rate, the full tow was guided through a series of baths by ABB motor controlled rollers pictured in figure 2.2 for washing and drawing. The godets pictured here control and drive the line speeds entering and exiting draw (v_0 and v_1).

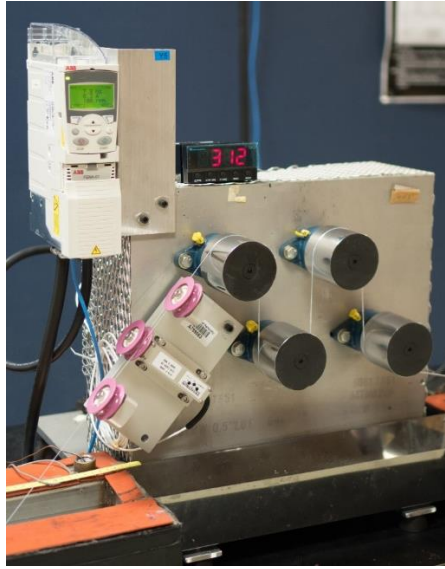


Figure 2.2 ABB electric motor controlled roller used to guide fiber along the spinline, variations in roller speeds generate draw.

Following coagulation, the fiber was passed through a 50 wt% DMAc/H₂O gel stretch bath and followed by four room temperature DI water wash baths, first stage draw in 90°C DI water, second stage draw in 160°C Glycerol, and two additional 90°C DI water wash baths. The tow was then pulled through a spin finish bath of 0.65 wt% silicone aqueous emulsion composition, passed over six heated rollers for drying, and wound onto a traversing collection spool.

2.1.4 Fiber Draw

Polymer dope was pumped through the spinnerette at 1.7 ml/min and pulled through the coagulation bath onto a godet roller with linear speed 0.91 m/s. The formed fibers were drawn after coagulation in a room temperature gel stretch bath at a DDR of 2.1 and washed at a DDR of 1.0 in each wash bath. The conditions outlining the experimental draw matrix, first stage hot water DDR₁ (90°C) and second stage hot glycerol DDR₂ (160°C) were increased or decreased depending on the DDR_{total} goal. Speeds at take-up were set to maintain a tension of 100g, to avoid added draw.

2.2 Results

The DDR sample points were spread throughout the experimental matrix and adjusted as the draw limit was approached and breaks were observed. Figure 2.3 shows the points of instability representing a complete break of tow for a combination of DDR_1 and DDR_2 values to form the draw limit of fiber draw in first and second stage draw. A linear fit of these values represents the draw limit and was quantified as an average of the combined DDR_{total} values.

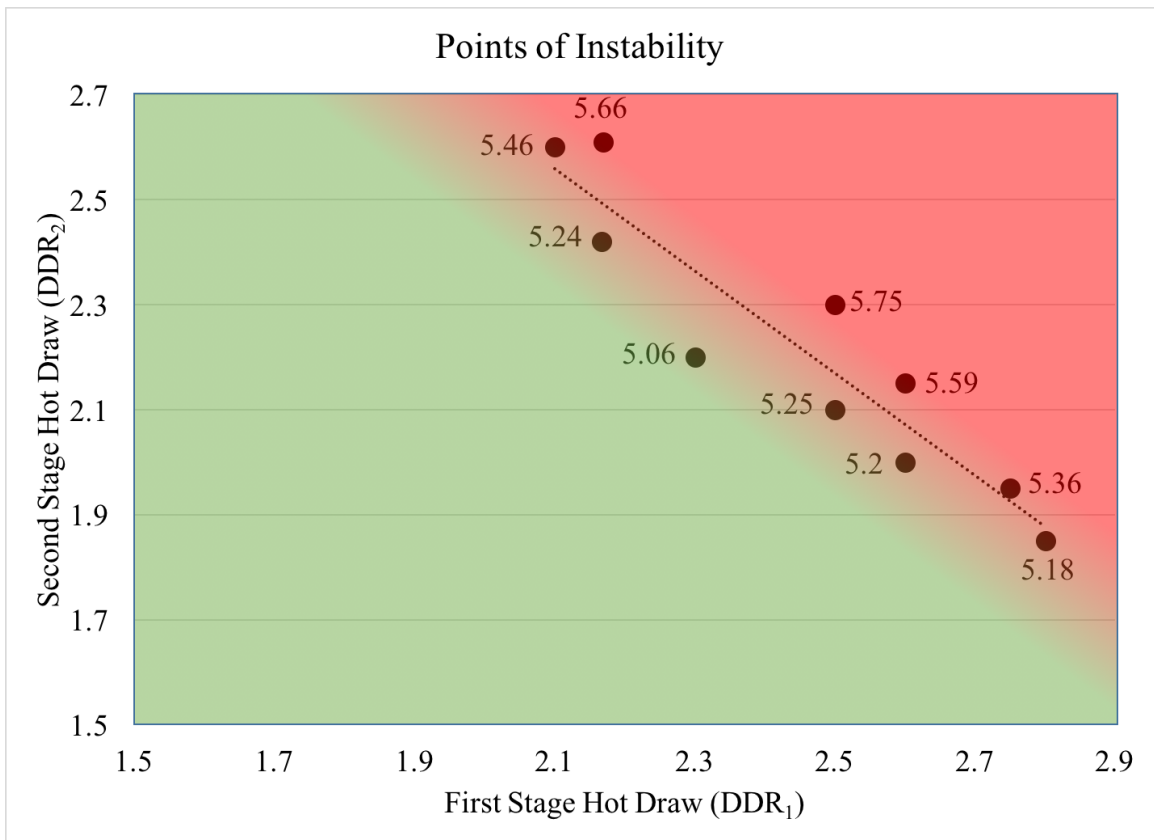


Figure 2.3 Graphic representing the DDR_{total} draw limit values (data labels) in terms of DDR_1 and DDR_2 .

As previously mentioned in the methods section, it was the goal to represent the draw limit of DDR conditions in hot draw as a single combination value, DDR_{total} . Each unstable breaking point was plotted in the points of instability figure 2.3 where a clear limit of first and second stage draw is shown. The draw limits of DDR_1 and DDR_2 is visibly represented

as an inversely proportional linear trend line. That is, as one stage of DDR is increased, instability occurs at lower DDR in the other stage of hot draw. The first and second stage hot draw limit can be quantified as a DDR_{total} value, where fiber was unstable and resulted in a break of the tow was determined to be 5.38 ± 0.23 , $N=10$. The average unstable DDR_{total} value found in this study provides a single numerical value of DDR_1 and DDR_2 combination values that form the unattainable limit theorized by the Deborah number. Maintaining first and second stage $DDR < 5.15$ will reduce the chance of instability in the line when using a multistage hot draw.

2.2.1 Observations during spinning

2.2.1.1 Visible Fiber Quality

Inching closer to the DDR_{total} draw limit, it was observed that the visible fiber quality was declining with increasing draw. Figure 2.4 shows a sample spool drawn at $DDR_1= 1.85$ and $DDR_2= 2.7$ for a DDR_{total} of 5.0, where spinning was stable for ten minutes.

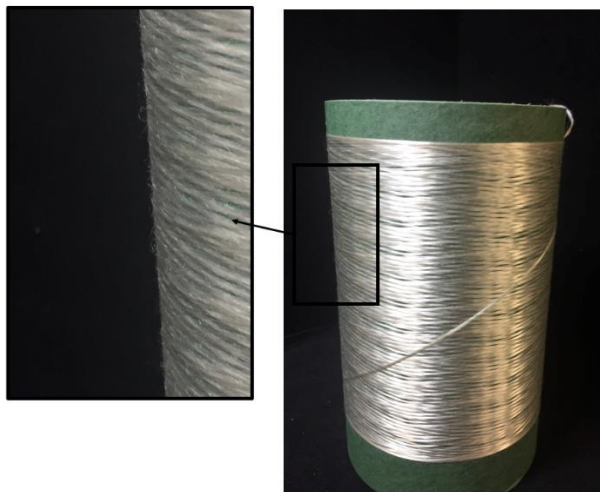


Figure 2.4 “Fuzzy” fiber indicated by broken filaments resulting from high DDR_{total} values at the edge of the draw limit.

(From these conditions, DDR_2 was increased to 2.8 to produce a break and a data point for the draw limit.) The fiber shown in the figure was drawn at settings on the edge of the draw

limit where the fiber diameter was being reduced to the point of breaking. The poor quality of the fiber is due to an increased fraction of individual broken filaments in the tow, presenting a fuzzy-like tow that with continued draw, will cumulate to a fully broken fiber tow. These visual observations demonstrate the mechanism that led to a complete break of fiber as draw increased. Thinning fiber diameter to a point where the cross-sectional area is not large enough to support the tensile load exceeds the break strength of the fiber tow and results in a break. Tow breaking at DDR_{total} beyond the draw limit was not an instantaneous break, but resulted after sufficient filaments broke to reduce the total cross-sectional area to a point that could not support the tensile load being applied. Quality precursor PAN fiber should maintain continuity and uniformity with no broken filaments throughout the spinning process to be used carbon fiber manufacturing.

Fiber presenting broken filaments was not the only indication of a probable fiber tow break. Beyond what can be visually observed, fiber properties and structure were changing significantly with draw, even at the lower DDR_{total} values.

2.2.1.2 Line Tension Monitoring

At the UK CAER solution spinning line, line tensions are monitored using a Tensitron Platform Mounted Fiber Transducer measurement system (Tensitron, Inc. Longmont CO, USA). The signal is converted to a tension reading displayed in grams-force as shown in figure 2.2. Tension measurements are a good indication of conditions on the line. While tensions are necessary in areas to create draw, very high tensions will result in poor fiber quality and potentially lead to failure.

Tensions are measured after coagulation, before and after first stage hot draw, after second stage hot draw, and before take-up. These are the regions where draw is applied to the fiber, tensions are highest, fiber properties are changing, and breaks occur most often.

Quantifying the tension readings corresponding to the draw limit can prevent defects that lead to “fuzzy” fiber shown in figure 2.4 and maintain stable processing conditions.

The tensions logged during the varying of first and second stage hot draw are shown in Figure 2.5. The details of first and second stage draw and resulting process stability are in Table 2.2.

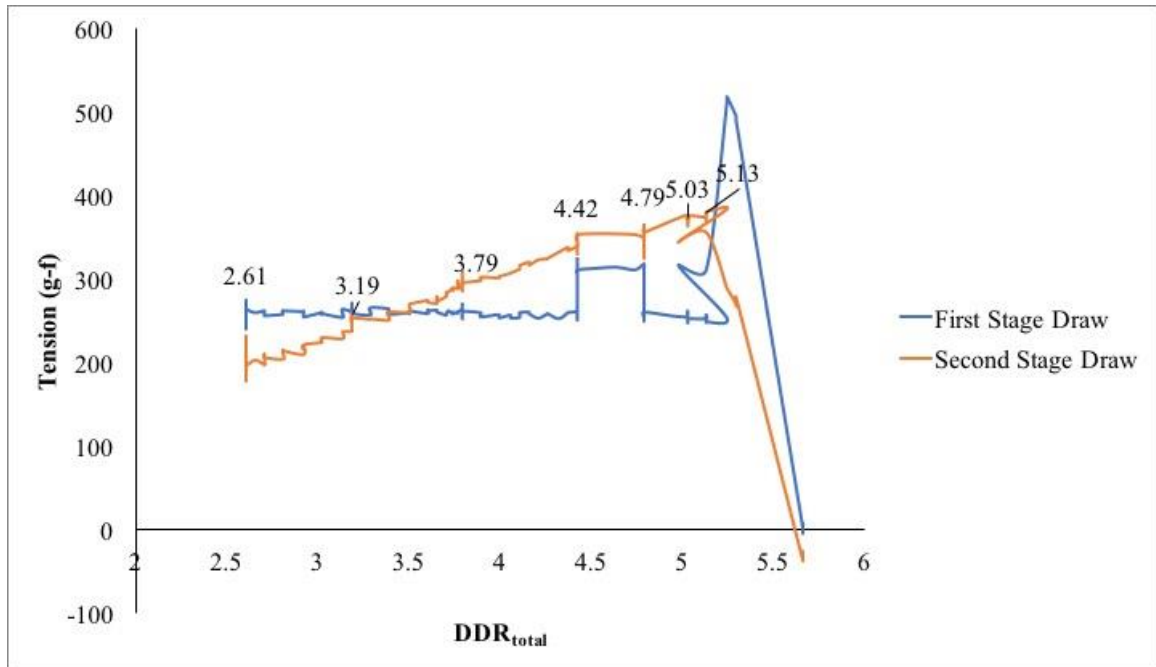


Figure 2.5 shows the recorded tensions at first and second stage draw plotted against hot DDR_{total} obtained in the investigation of the draw limit.

Table 2.2 Stable draw down ratios for first and second stage draw shown in figure 2.5

DDR1	DDR2	DDRtotal
2.00	1.30	2.61
2.00	1.59	3.19
2.00	1.89	3.79
2.00	2.21	4.42
2.00	2.39	4.79
2.00	2.51	5.03

The data found from tension measurements shows breaks occurring after the draw limit as erratic behaviors in the data develops. The tension measured before a break in second stage hot glycerol draw was 350 g-f. These values provide an additional way to quantify the limit of draw in terms of output during spinning in comparison to the user input DDR values. Maintaining tension below 350 g-f in second stage will prevent defect formation and breaks in this draw bath.

2.2.2 Microscopy

The fiber geometry and microstructural changes accompanied with fiber draw were investigated using scanning electron microscopy (SEM). Figures 2.6 and 2.7 show the diameter changes the fiber experiences in draw. The fiber diameter out of coagulation at 25 μm is reduced to 9 μm with first and second stage hot $\text{DDR}_{\text{total}} = 3.18$. Figure 2.7 shows the cross-sectional area comparison before and after hot draw, here fiber cross sections have decreased by nearly two-thirds. The diameter changes have a great effect on the modulus and break stress, properties that largely dependent on cross sectional area.

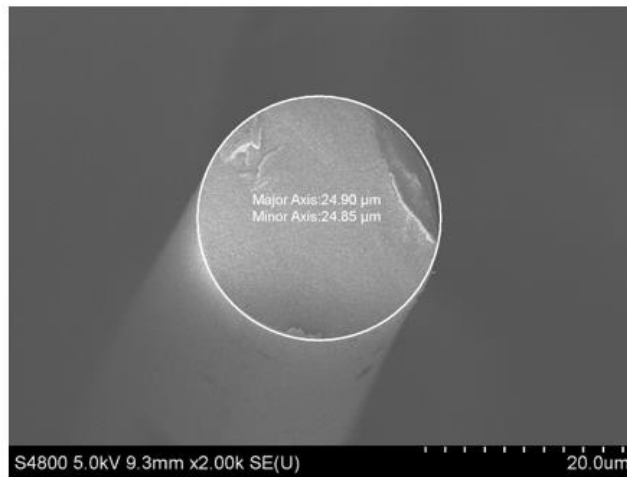


Figure 2.6 Cross sectional 2k mag view of fiber right out of coagulation pre-hot first and second stage draw.

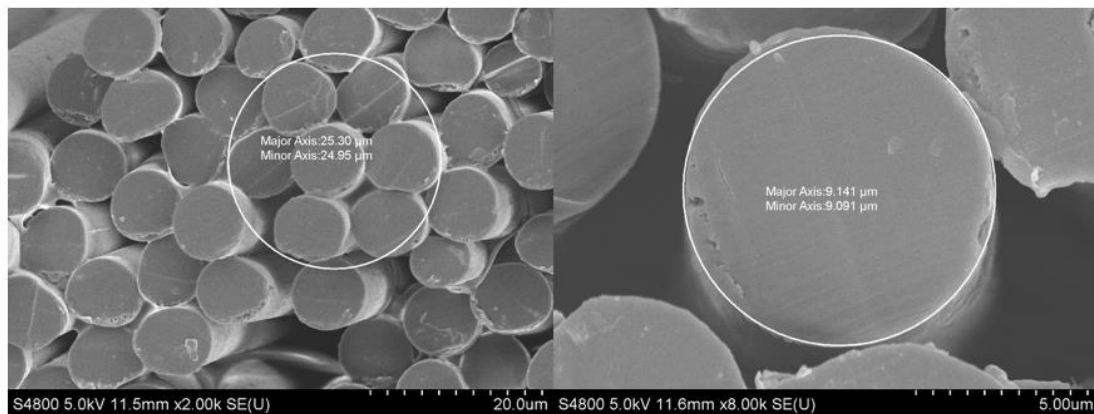
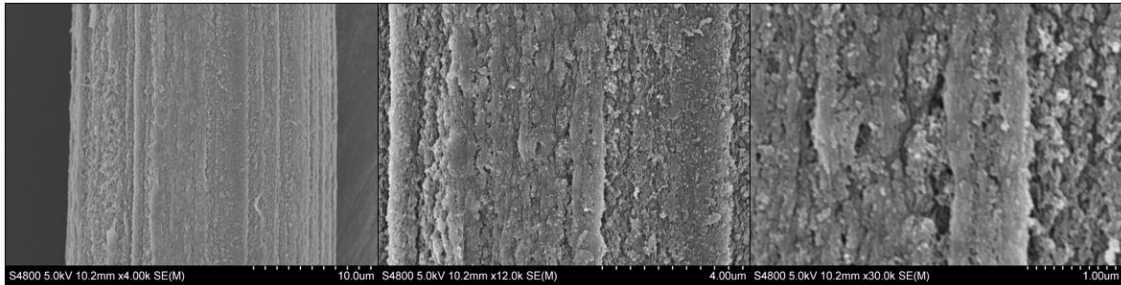
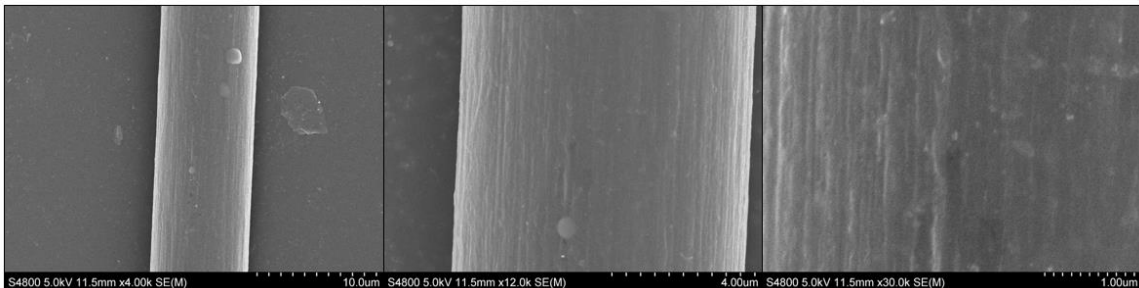


Figure 2.7 Fiber post hot first and second stage $\text{DDR}_{\text{total}}=3.18$ draw at 2k high mag (left) 8k high mag (right).

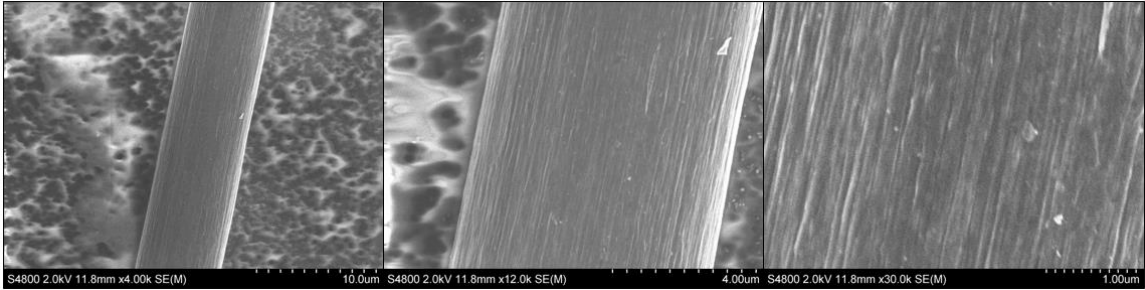
Additional images of stable fibers collected in this study are shown in figure 2.8. The images show the microstructural effects of draw. The fibrils comprising the filaments are shown as striations along the axial direction in each set of figures. Pre-hot drawn fiber, collected at the roller after coagulation is shown in (i). Immediately collected after solvent exchange, the filaments have a rough surface appearance from the formation of the porous structure of the fibril structure and have very low orientation with the axis. In hot draw conducted at temperatures above T_g , the polymer chains in the fibrils begin to relax and align in the direction of tension [31]. This alignment results in the closing of gaps or pores in between these structures and an increase in density of the filaments. Shown in (ii), the fibers have been subjected to hot $DDR_{total} = 3.18$, the striations are much smoother and the porous structure is less clear than in (i). Figure 2.8 iii. shows the post carbonized (ii) fiber, here the fibrils are more distinctive and the surface is less smooth from the loss of non-carbon elements and amorphous regions. The transition from a smooth surface to a more defined, striated structure during mass loss will intensify any voids or defects in the fiber and ultimately decrease the break stress of the fiber.



(i)



(ii)



(iii)

Figure 2.8 Side view SEM images of PAN (i) fiber out of coagulation, pre-hot draw (ii) precursor fiber post hot $DDR_{total}=3.18$ (iii) Carbonized fiber post hot $DDR_{total}=3.18$.

2.2.3 Scale

It is obvious that the spinning parameters and fiber characteristic goals in industry will not be equal to those in this study. A fiber spinning setup with diameters differing from this study can be adjusted using the equation for the change of diameter with respect to DDR is shown in equation 2.5. This relationship demonstrates that the hot DDR_{total} draw limit for instability that was found in this study may not be the limit for a larger fiber tow or larger diameters of single filaments, but may be scaled to fit other spinning conditions. Full derivation of this equation can be found in Appendix A.

$$\frac{d_{in}^2}{d_{out}^2} = DDR \quad [2.5]$$

Equation 2.5 assumes no necking, constant volume with draw increase, and shows the relationship between diameter change and DDR. For fiber diameters deviating from those of this experiment, DDR_{total} can be found using the methods described previously. These calculations allow for the experimental methods to be scaled for use in an industrial setting for a desired final fiber diameter.

2.3 Conclusion

In this study, a limit to hot multi-stage draw was found and quantified as a single value representing the total hot draw as a combination of first and second stage DDR. This value gave an experimental value to the Deborah number, used in theoretical modeling of viscoelastic flow with draw. It was observed that the visual quality of the fiber began to diminish as conditions approached these values, suggesting parallel effects on the properties of the fiber, affected directly by the structure of the fiber.

Intact fiber samples from stable DDR_{total} conditions were collected for further characterization and investigation of the effects of draw on the performance of the fiber. The coming chapters will explain the experimental methods and results of these characterization techniques to relate process conditions (in the form of DDR_{total} found in the draw limit study) to fiber properties and structure.

Chapter 3. Mechanical Properties and Microstructure Approaching the Draw Limit

3 Introduction

In industry, PAN fiber is typically collected at take-up speeds in the range of 200 m/min [32]. In a process this fast, fiber quality control is mostly performed during spinning by monitoring line tensions and temperatures as well as observation of fiber at take-up. The study in chapter two detailed the process of taking DDR at first and second stage hot draw to their limits. There, defects in the fiber reached the point of visibility in the form of broken filament and “fuzzy” fiber and ultimate failure of the entire 500 count filament tow. However, most defects in the fiber microstructure that weaken the material develop far before they are visually detectable. This study will dive deeper into the effect of first and second stage hot draw, to the micro and atomic level of the fiber structure. Results will aid in the investigation of the processing/structure/property relationship and quality control of PAN precursor fiber spinning and the effects on the resultant carbon fiber.

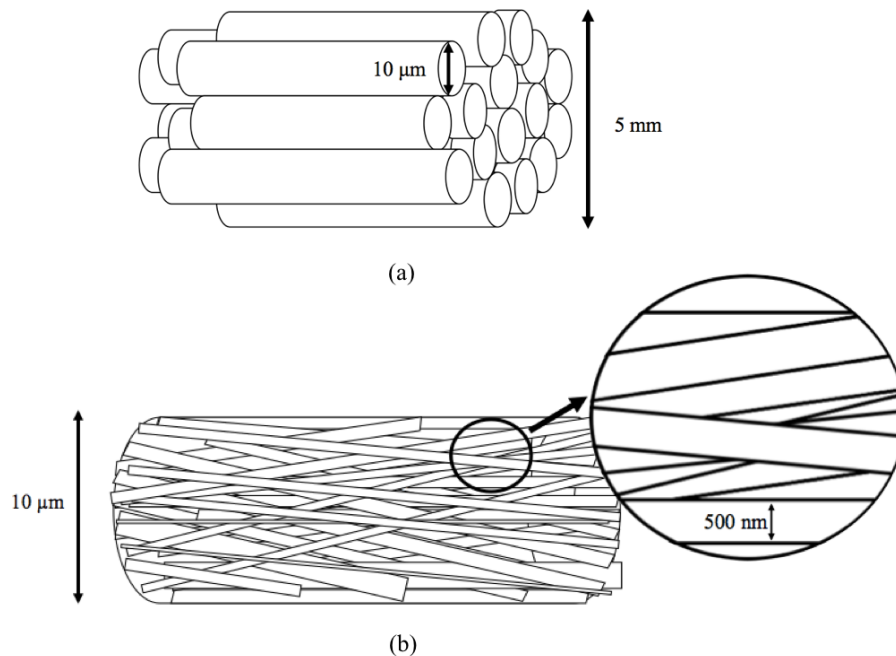


Figure 3.1 Visual representation of (a) 500 filament count fiber tow, (b) Individual filament fibril microstructure.

The visual effects of draw on fiber were observed during spinning as the tow thinned, decreased in diameter, became fuzzy or completely broke. Defects on the individual

filaments include voids in the microstructure and surface flaws. Even further, the crystalline structure of the fibrils, nanoscale subdivisions of individual filaments, can affect the performance of the fiber. Figure 3.1 shows a comparison of the size scale of a fiber tow, filament, and fibril.

Multistage hot draw is used in fiber spinning to customize fiber dimensions and degree of orientation via elongation with the fiber axis. Along with these dimensional changes, densification of the filaments occurs as the porous structure, imparted during coagulation, formed by space between fibrils, begins to collapse. The effects of these can be seen in the mechanical properties and used as a tool to customize the fiber performance and potential for thermal conversion to carbon fiber. Also affecting mechanical properties, the degree of orientation of the crystal structure with the fiber axis results from draw.

Scanning electron microscopy (SEM) was used to image the macroscopic geometry and surface of individual filaments. Ultrasonic frequency resonance of a single filament was used to determine the fiber linear density (and thus diameter), and single filament tensile testing was used to quantify the tensile strength and modulus of the fiber. To investigate the crystal structure, specifically crystallite sizes and degree of crystal orientation, wide angle x-ray diffraction (WAXD) studies were performed on the fiber.

The combination of these techniques characterized the fiber properties and related the crystalline structure to mechanical performance up as a function of the experimentally determined draw limit. PAN precursor fiber samples collected were thermally converted to carbon fiber and both materials were characterized using single filament tensile testing and WAXD.

3.1 Mechanical Properties

The structure-property relationship of polymeric fiber is one that has been studied previously [12, 21, 23, 24, 26, 32-35]. It is well understood that draw is needed in solution spinning in order to align PAN's structure with the axis and create a more dense material, leading to an improvement in mechanical properties [36]. However, draw is not infinite and there are limits to this mechanism and studies by Gupta et al.[37] suggest a decrease in performance with excessive draw. To study the effects of draw limits on the mechanical

performance of fibers, samples were tested in tension. The resultant stress associated with draw can be explained by modeling the fiber as a long cylinder in the fundamental equation for tensile stress in equation 3.1.

$$\sigma = \frac{F}{A} \quad [3.1]$$

Shown here, for a constant cross sectional area (A) or fiber diameter, as the draw force increases (F), more tensile stress (σ) is experienced by the fiber. However, draw decreases the diameter of the fiber while simultaneously densifying the cross section as voids, formed earlier in the spinning process, collapse. This creates a fiber that experiences more stress for a given tensile force, increasing modulus as shown in the equation for Young's modulus of elasticity (eq 1.4.3). With little or no draw, there is no tensile force to collapse voids, leaving a porous structure.

The effects of voids on fiber performance can be determined by relating single filament tensile testing data to the increase in draw. The number of voids decreases as pores collapse with increasing draw. Information such as tensile strength or break stress (σ) and Young's modulus of elasticity (E) is used to quantify the strength and stiffness of the material. Break stress, sometimes referred to as ultimate tensile stress, is the stress corresponding to ultimate failure. Young's modulus of elasticity can be related to the relative stiffness of a material and is the ratio of stress to strain. The understanding of the hot draw relationship to the modulus and break stress of PAN as a precursor material can result in controlled optimization of precursor for the production of carbon fiber.

3.1.1 PAN Fibers

The resultant properties of carbon fiber rely on the processing of PAN fiber. The effects and limits of hot draw in PAN precursor processing will be determined in the following.

3.1.1.1 Tensile Testing

Samples for mechanical testing of PAN precursor fiber were collected at stable-processing spinning conditions from take-up when determining the limits of draw described in chapter two. Samples past the draw limit were obtained from spooled fiber collected during the 10-minute change over period for establishing stability. The DDR values for the mechanical testing samples are shown in table 3.1.

Table 3.1 First and second stage DDR values for each fiber sample that was characterized in this study.

DDR Values for Characterization		
DDR₁	DDR₂	DDR_{total}
2.00	1.30	2.60
2.00	1.59	3.18
1.95	1.70	3.32
2.09	1.60	3.34
1.95	1.90	3.71
2.00	1.89	3.78
2.09	1.85	3.87
2.00	2.21	4.42
2.61	1.80	4.70
2.00	2.39	4.78
1.78	2.80	4.98
2.61	1.99	5.19
2.00	2.60	5.20
2.42	2.17	5.24
2.61	2.17	5.66

Single filament tensile testing of the collected PAN precursor fiber samples was conducted using a Textechno FAVIMAT+ with (AI)ROBOT2 equipped with auto feed. Values for stress at break (tensile strength) and Young's modulus were calculated and reported by the instrument for testing parameters outlined in ASTM D3822 (Standard Test Method for Tensile Properties of Single Textile Fibers).

Each PAN precursor sample test consisted of three full magazines ($N \geq 75$) of 25.4 mm (1 inch) gauge length fibers. Axial force on the specimens was measured until break using a 210 cN (214.14 gf) load cell for a cross head speed of 5 mm/min and a pretension of 0.50 cN/tex (0.0566 g/den), a textiles unit for tenacity measuring the break stress of a fiber.

The apparatus also performed linear density measurement and diameter (D) calculations. 25.4 mm (1 inch) gauge length single filament precursor fiber samples were brought to a 0.5 cN/tex pretension at 1 mm/min crosshead speed for resonance frequency measurement. Linear density values calculated by Favimat+, user provided bulk density material values (ρ), and equation 3.2 were used to calculate fiber diameter (D) for fibers with circular cross sections. Diameter and measured force were then used to calculate break stress (equation 3.1) by the Favimat+ tensile testing instrument.

$$Linear\ Density = \frac{\rho V}{l} = \rho A = \rho \frac{\pi}{4} D^2 \quad [3.2]$$

Table 3.2 The reported precursor values [31] and carbon fiber values obtained via Helium Pycnometry at UK CAER for bulk density were used by the Favimat+ to report diameter.

Bulk Density Values	
Material	ρ
PAN Precursor Fiber	1.18 g/cm ³
Carbon Fiber	1.76 g/cm ³

Favimat reported diameters, break stress, and modulus values of various commercially available carbon fibers were authenticated by data sheet comparison before testing the samples collected from these experiments.

3.1.2 Carbon Fibers

The measurement and quantification of the strength of PAN precursor fiber is important for thermal conversion to carbon fibers with the properties desired for high strength applications. PAN precursor fibers have reported strength values from 0.5-1.0 GPa and modulus 18-20 GPa [23] and increase after carbonization to 5-6 GPa and of 250-400 GPa [3, 12]. The investigation of thermally converted PAN fibers is important for this study to fully understand the effect of draw in PAN fiber spinning on the resulting materials intended for use in carbon fiber composites. To obtain a processing/structure/property relationship through the full conversion process of precursor to carbon fibers, testing methods performed on precursor fibers were repeated on resultant carbon fibers.

3.1.2.1 Thermal Conversion to Carbon Fiber

Thermal conversion of precursor fiber to carbon fiber requires carefully controlled time and temperature conditions. The conversion process was conducted in two steps, stabilization and carbonization. Each sample was converted using the same conditions to maintain orientation formed during spinning for a fair comparison. PAN precursor fiber was unspooled onto a constant length (11 cm) aluminum frame to a ten-wrap fiber hoop for stabilization. Fiber was heated in an LND series Despatch convection oven (LND 1-42-3) at a controlled temperature ramp reaching 150-300°C for several hours to oxidatively stabilize the fiber.

Sample hoops from stabilization were mounted at the same length on a graphite hanger with constant force across all samples for carbonization. Samples were ramped in a Thermal Technology High Temperature Furnace (1000-2560-FP20) purged of air to high temperatures upward of 1200°C in high purity Helium for tens of minutes, after which they were ready for characterization.

3.1.2.2 Tensile Testing

PAN precursor samples collected and thermally converted to carbon fiber were also tested for break stress and Young's modulus of elasticity using the same Textechno FAVIMAT+ with (AI)ROBOT2 equipped with auto feed.

Testing methods for carbon differ slightly from precursor fiber to obtain system compliance with the measurement of multiple fiber gauge lengths. Individual carbon fiber filaments at gauge lengths 25.4 mm, 35.4 mm, 45.4 mm, and 55.4 mm were measured for resonance frequency (diameter) at 2 mm/min crosshead speed to a pretension value of 1.0, 1.5, 2.0, 2.5 cN/tex respectively. Tensile testing was performed for gauge lengths 25.4 mm, 35.4 mm, 45.4 mm, and 55.4 mm ($N_{\text{total}} \geq 40$, 10/gauge length) at test speeds predetermined to result in a ~30 second break at 0.50 cN/tex pretension.

3.1.3 System Compliance

Carbon fiber requires the use of different mechanical testing and analysis methods. Due to the high stiffness of carbon fibers, system compliance must be performed to obtain corrected modulus values. The system elongation (primarily load cell elongation) is negligible compared to the large elongations of PAN precursor fiber and therefore compliance correction is not necessary for precursor fiber.

High modulus carbonized PAN fibers are more resistant to strain when subjected to a tensile force. This results in difficulty measuring elongation at break with tensile testing instrumentation and thus difficulty calculating modulus. The spring constant of the instrument clamp and load cell system is of the same magnitude as the fiber and contributes error to the modulus data [5]. To correct this error, a system compliance must be determined for the instrument's spring constant and subtracted to adjust raw modulus data. The correction value (C_s) for system compliance is determined using the relationship of stress/strain data collected from tensile testing filaments at a range of gauge lengths. Carbonized fibers were tested at 25.4 mm (1 inch), 35.4 mm, 44.4 mm, and 55.4 mm gauge length. The average indicated compliance (C_a) (equation 3.4) is calculated using data reported by the Favimat+ system and then plotted against each corresponding gauge length. Extrapolation of the resulting linear relationship from the plot yields system compliance (C_s) at the Y-intercept. To correct reported values of modulus (E_a), the corrected compliance value (C) must then be calculated for each gauge length using equations 3.3 and 3.5.

$$C = C_a - C_s \quad [3.3]$$

$$C_a = \frac{l_0}{E_a \times A} \quad [3.4]$$

A = Cross sectional area of specimen

E_a = Average reported modulus

l_0 = Specimen gauge length

C = Corrected compliance

C_a = Indicated compliance

C_s = System compliance

The corrected value for modulus ($E_{corrected}$) at each gauge length can then be calculated using equation 3.5.

$$E_{corrected} = \frac{l_0}{C \times A} \quad [3.5]$$

3.1.4 Weibull Analysis

As PAN fibers are converted to carbon fibers, most non-carbon elements are removed, nearly 50 percent of the mass is lost, [22] resulting in reduction of diameter (~40 percent), and the material becomes more brittle. This loss of mass combined with the extreme processing conditions during conversion leads to formation of defects in the material [3]. Defects that form in carbon fibers during thermal conversion greatly affect the mechanical performance of the material [38] and lead to large variations in reported break stress. Weibull analysis is conducted to quantify these variations and gives insight into the distribution of flaws in the fibers that result in failure.

A two parameter Weibull statistical distribution of combined break strengths at 25.4 mm, 35.4 mm, 45.4 mm, and 55.4 mm gauge lengths was used to obtain a Weibull distribution of the break probability.

$$F = \frac{R}{N+1} \quad [3.6]$$

The probability of failure (F) under a given stress for the number of fiber breaks (R) in a population (N) is shown in 3.6. This value in combination with the linear regression of 3.7 are used to determine the Weibull modulus (m). The slope of the linearized 3.7 (shown in 3.8) is the Weibull modulus, representing variation in reported break stress values. A larger m indicates lower variation. Scale parameter (σ_0) is the characteristic stress which relates the characteristic strength to the characteristic length and is found using the values from

3.8 and equation 3.9. The Weibull modulus (m) and scale parameter (σ_0) are then used to calculate $F(\sigma)$ the Two-parameter Weibull distribution (3.7). $F(\sigma)$ is plotted against all reported break stresses to obtain a Weibull failure probability curve for stress.

$$F(\sigma) = 1 - \exp \left[- \left(\frac{\sigma}{\sigma_0} \right)^m \right] \quad [3.7]$$

$$\ln \left[\ln \left(\frac{1}{1-F} \right) \right] = m \ln \sigma - m \ln \sigma_0 \quad [3.8]$$

$$\sigma_0 = \exp \left(\frac{-y_{int}}{m} \right) \quad [3.9]$$

The data is presented in a 0-100 percent probability of failure against a range of measured break stresses. The S shape of this curve gives a visual representation of the Weibull modulus. A wider S curve represents a large variation and a thinner S curves represents smaller variations in break stress and thus fewer defects per unit length in the material.

3.1.5 Results

The following details the results of single filament tensile testing on PAN precursor fiber and subsequent carbon fiber samples at various hot DDR_{total} in solution spinning. Mechanical performance is compared with hot DDR_{total} spinning parameters in figures 3.2-3.5. The mechanical performance has been quantified in the form of break stress or tensile strength (σ) and Young's modulus (E), two properties that influence the performance of precursor and resultant carbon fiber.

In chapter one, a limit was found for fiber spinning stability in first and second stage hot draw, beyond which filaments began to break and spinning conditions were deemed unstable. Here, we investigate the effects and possible limitations of draw on the improvement of mechanical performance of the fiber. A complete data set from single filament tensile testing is reported in Appendix B.

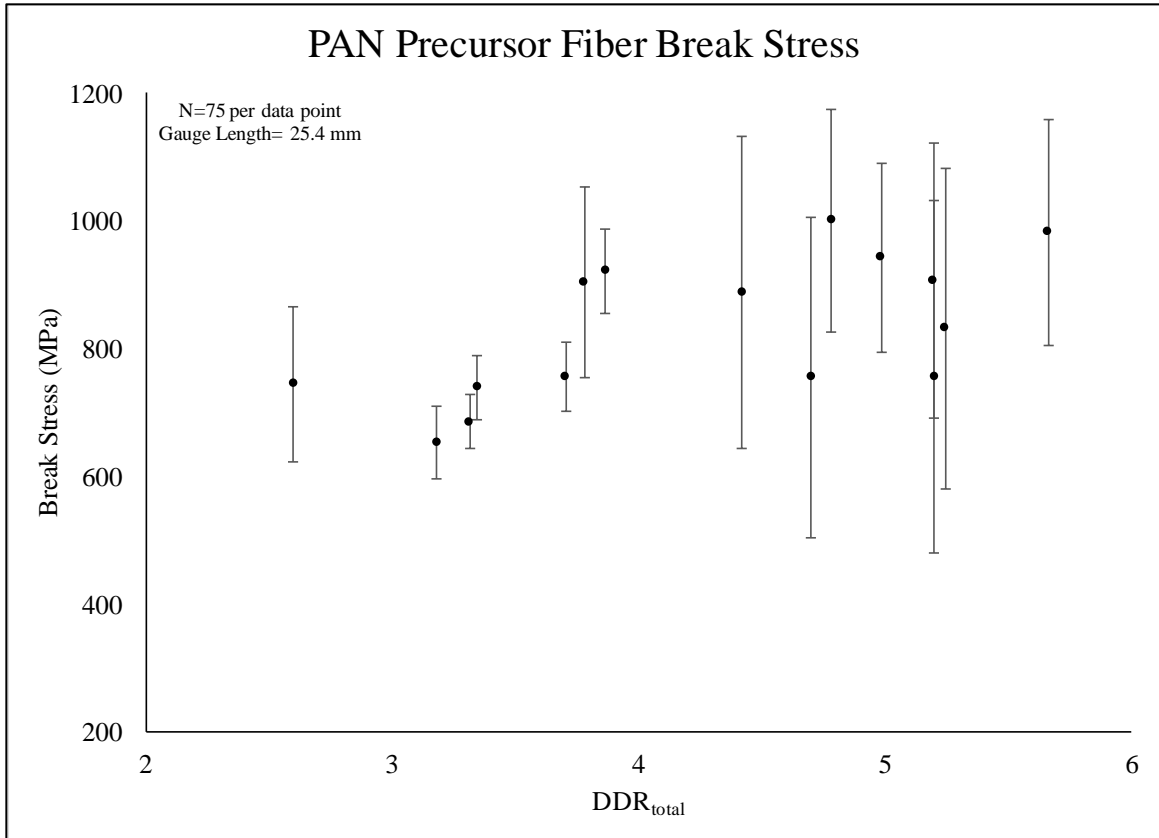


Figure 3.2. Plot of average PAN precursor fiber break stress vs. DDR_{total} of ($N > 75$).

At low DDR_{total} values, break stress increases with increasing draw and variation is small for PAN precursor fiber. As the draw approaches the draw limit of $DDR_{total} = 5.38 \pm 0.23$, shown as a red line in figures 3.2-3.5, the deviation become large and the correlation is lost. The increase in variation can be visualized during spinning at these high draws as “fuzzy” fiber.

The resultant carbon fiber break stress relationship to draw is plotted in figure 3.3. The relationship shows again, as draw increases, the break stress of the resultant carbon fibers continues to increase past the draw limit.

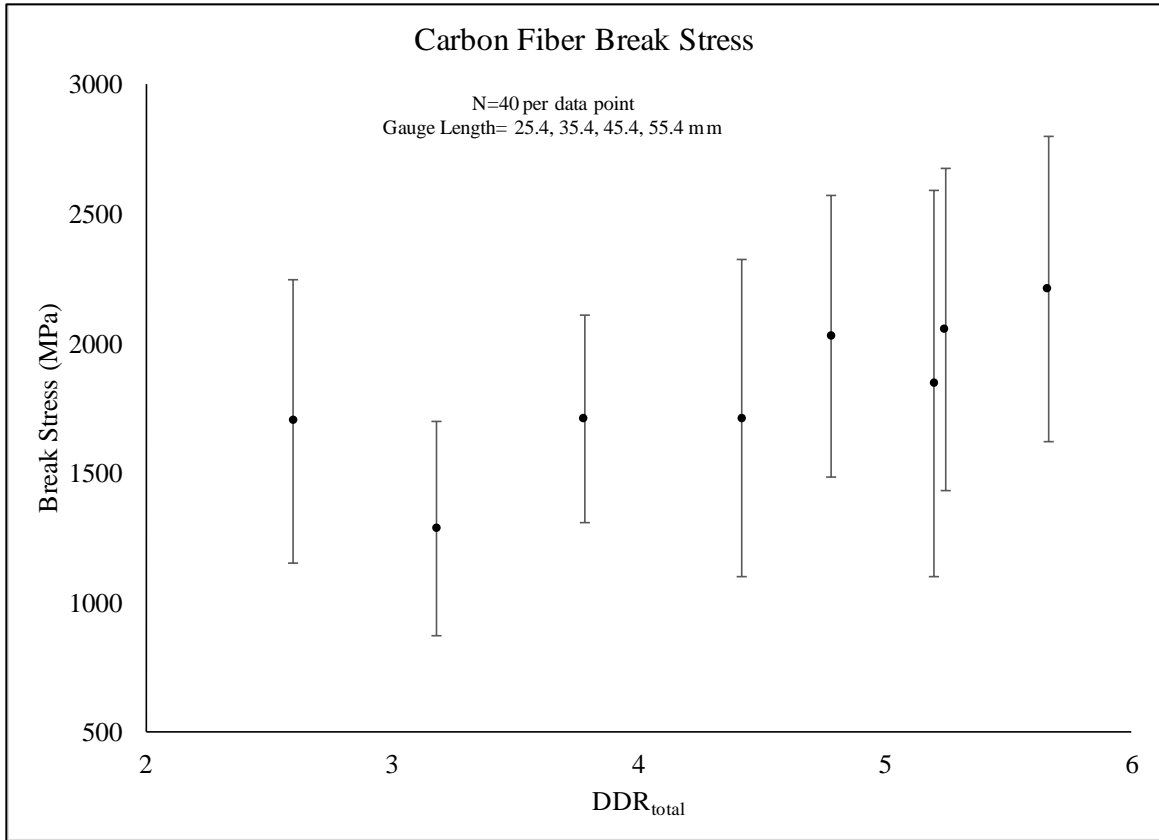


Figure 3.3 Plot of average resultant carbon fiber break stress vs. DDR_{total} ($N \geq 40$).

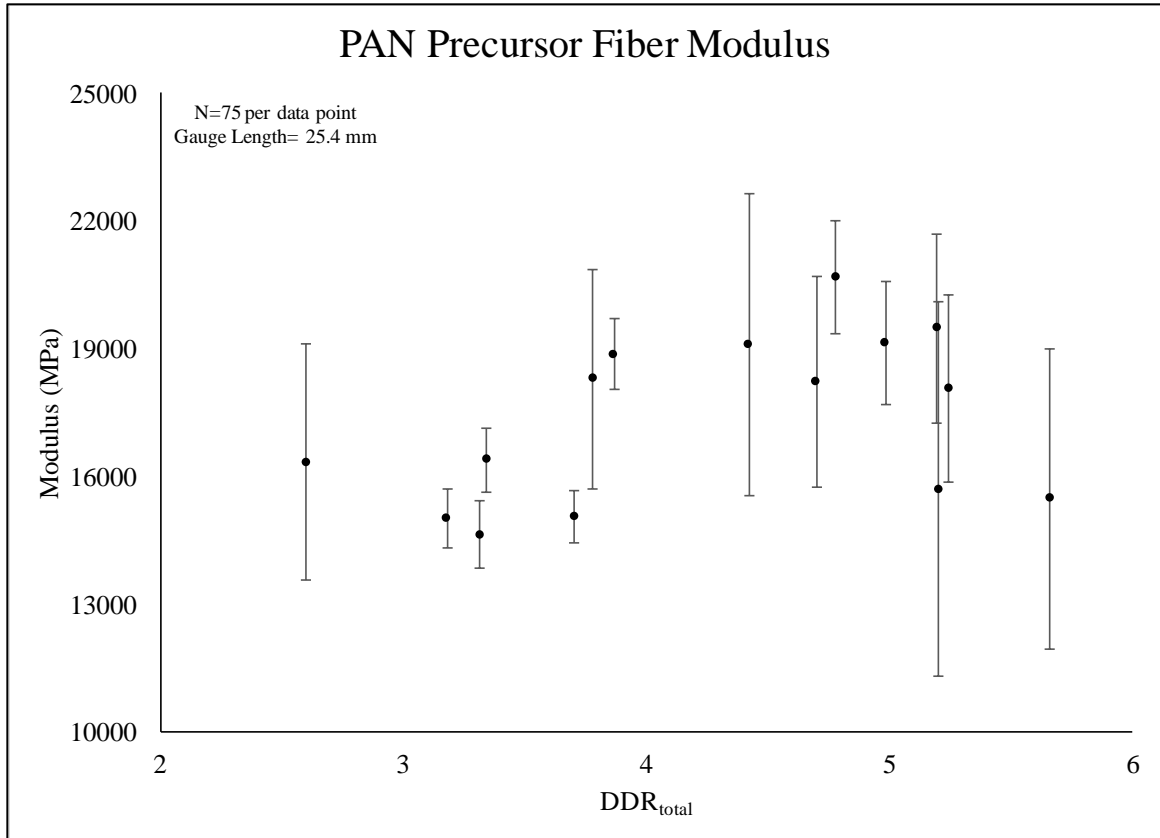


Figure 3.4. Plot of average PAN precursor modulus vs. hot draw DDR_{total} ($N \geq 75$).

Fiber modulus is dependent on microstructure and preferred orientation. The modulus values obtained from tensile testing PAN precursor and resultant carbon fiber are plotted against hot draw DDR_{total} in figures 3.4-3.5. PAN precursor moduli values are shown to increase with increasing DDR_{total} and reach a maximum before decreasing at the draw limit. The variation of modulus values is also low at lower DDR_{total} , but grows approaching the draw limit. These trends are similar to those of PAN precursor break stress with increasing draw.

Carbon fiber modulus, corrected for system compliance, also behaves similarly to its break stress as DDR_{total} values continue to increase with draw past the limit.

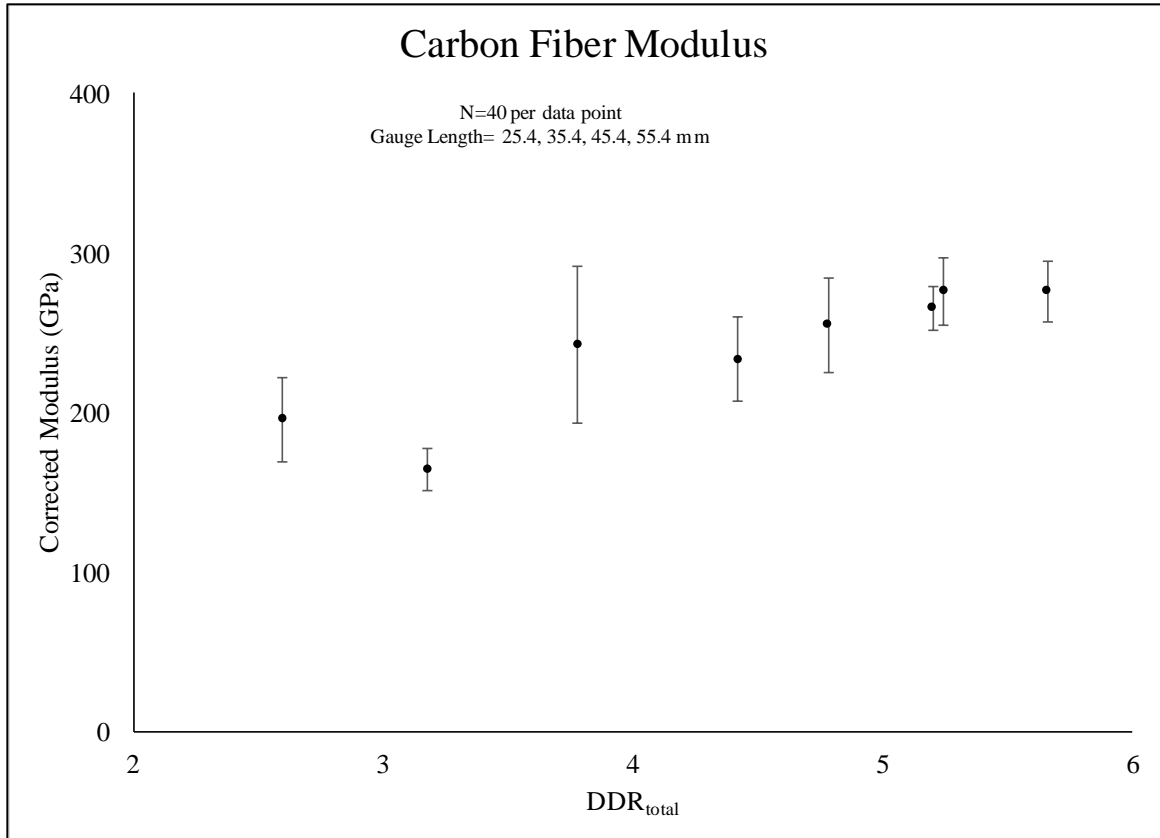


Figure 3.5 Plot of resultant carbon fiber corrected modulus vs. hot draw DDR_{total} .

Although the carbon fiber samples do not show a decline in properties past the draw limit in solution spinning, it is important to stay below this limit in PAN precursor spinning. Processing at or above the draw limit was determined previously to result in broken PAN precursor filaments which can decrease the handling quality of the material for further processing to carbon fiber.

During draw, diameter decreases and the fiber becomes more dense, with this, the probability for defects also decreases. Weibull analysis methods are often used to quantify the probability for defect initiated, brittle failure to a stress value [39]. Weibull modulus values and a full Weibull analysis of the carbon fibers in this study can be seen in table 3.3 and figure 3.6.

The Weibull modulus values in table 3.3 were calculated using the tensile testing data of carbonized PAN fibers drawn at DDR_{total} during solution spinning. As DDR_{total} increased, Weibull modulus increased and reached a maximum around the draw limit shown in red. Past the draw limit, Weibull modulus values decreased. Weibull modulus is used to

quantify the variation in break stress values, a higher Weibull modulus indicates a thinner distribution, less variation in break stress, and fewer defects that lead to premature breaks [38]. This suggests that as draw increased, the number of defects decreased but at the draw limit, the number of defects in the fiber and variation in break stress began to increase.

Table 3.3 Weibull modulus values for thermally converted PAN fibers for hot DDR_{total} obtained by linear regression of the equation for two-parameter Weibull distribution.

DDR_{total}	Weibull Modulus (m)
3.18	3.13
2.60	3.41
3.78	4.67
4.42	3.36
4.78	4.24
5.20	2.49
5.24	3.55
5.66	3.22

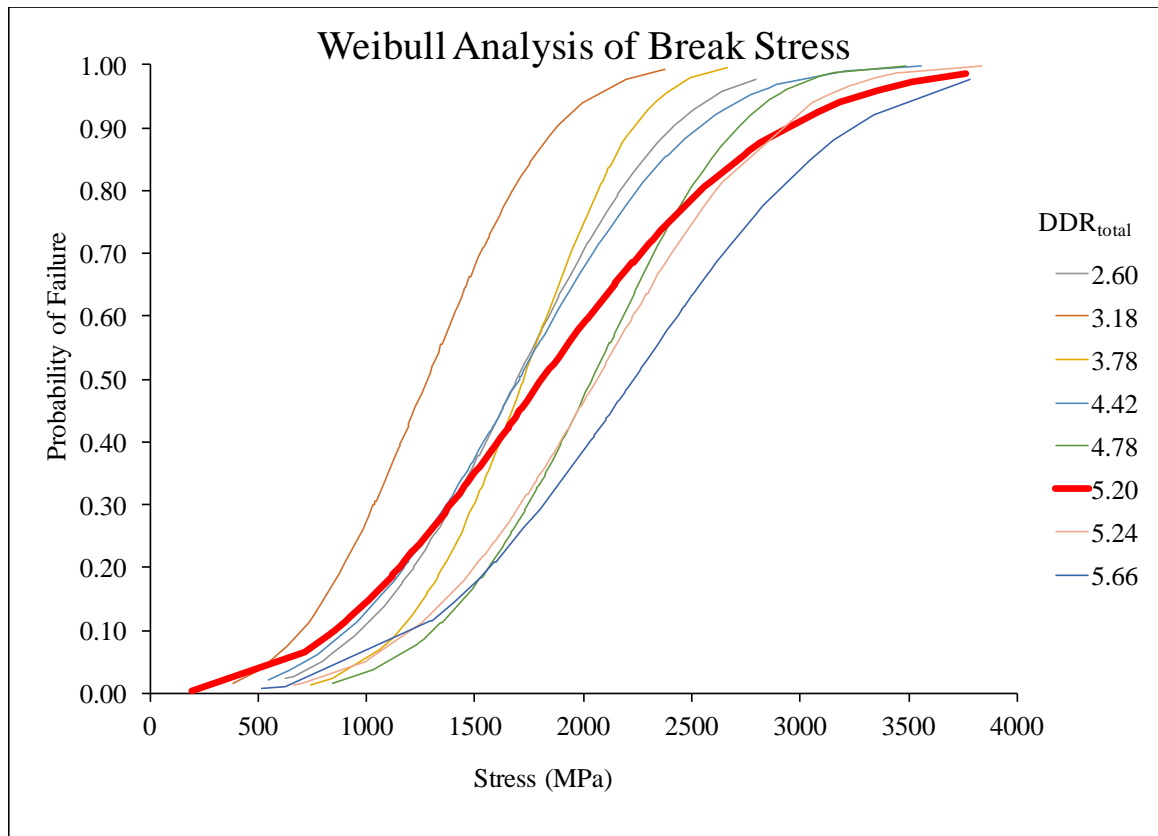


Figure 3.6 Distribution of failure probability vs. tensile stress using Weibull analysis ($N \geq 40$) for resultant carbon fiber.

The Weibull analysis plot shows the probability of failure for a range of stresses. Each curve is representative of a DDR_{total} in solution spinning. Figure 3.6 gives a visual for the conclusions made with the Weibull modulus values. Variation in break stress is larger for DDR_{total} values past the draw limit and at very low DDR_{total} and is represented as a wider S-curve distribution of break stresses. The curve in red shows the Weibull distribution of a sample collected past the draw limit, where variation is highest and the curve is widest. Investigating further into the individual effects of first and second stage draw, the results of tensile testing were plotted for each stage of draw in figure 3.7. Each plot shows the relationship between increasing draw in each stage of hot draw and mechanical testing data.

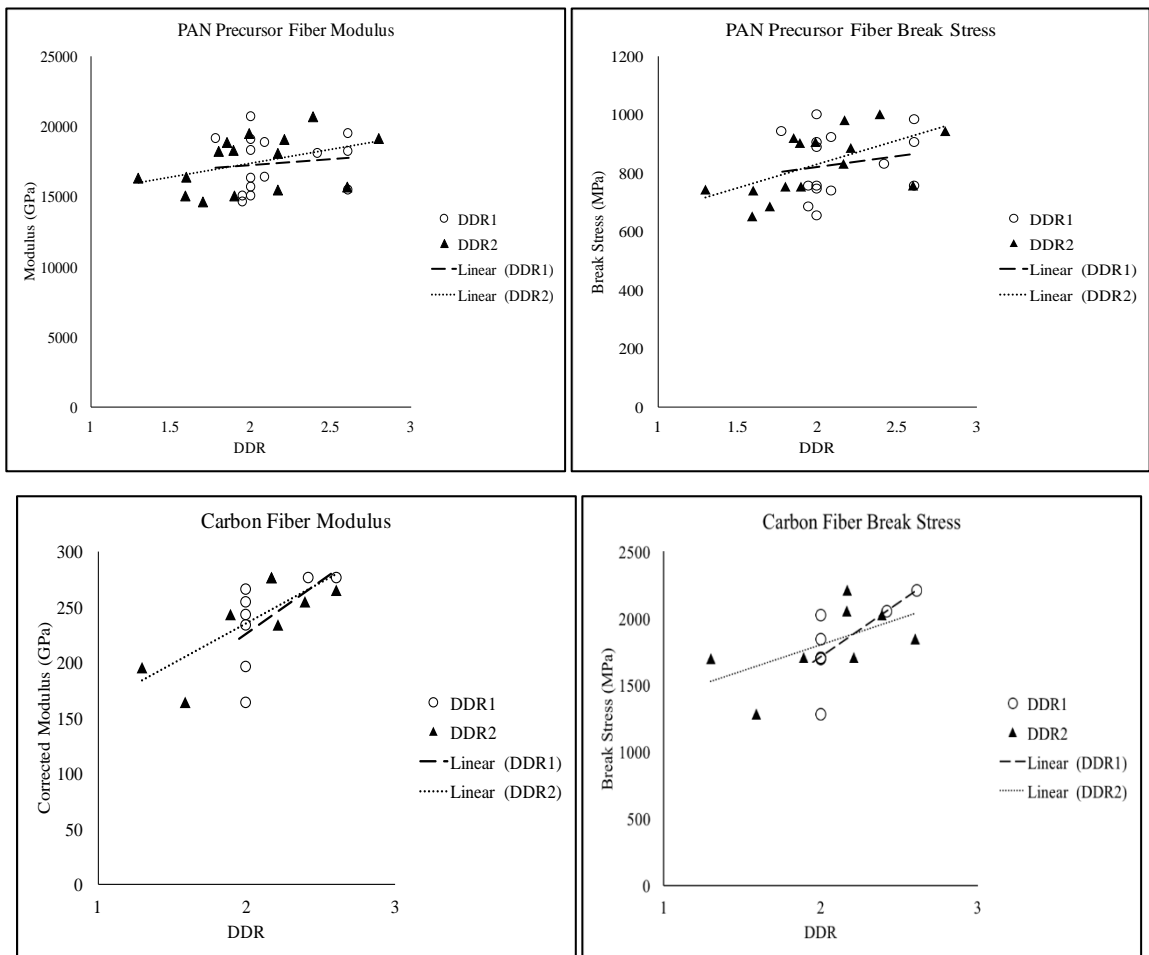


Figure 3.7. Weighted effects of first and second stage draw on the mechanical testing results. (From top left to bottom right, PAN modulus, PAN break stress, carbon fiber modulus, carbon fiber break stress.)

These results show that both modulus and break stress values show a larger increase with increasing DDR_2 as shown by the larger sloping PAN fiber trend lines. Carbon fiber plots show the opposite, that the mechanical properties increase more with increasing DDR_1 as shown by the trend lines. These plots show the weighted effects of each stage of draw with respect to the mechanical properties of the fiber samples. It can be concluded that the effects of draw in glycerol (DDR_2) are greater than draw in hot water (DDR_1) on PAN precursor samples. The conflicting results of the carbon fiber samples indicate that hot water draw (DDR_1) has a larger effect on the resultant carbon fiber mechanical properties than in glycerol (DDR_2).

Break stress trends in the tensile testing data were explained by defects in the fiber and cross sectional structure. Fiber moduli however, depends more on the microstructural properties and composition of the fiber than defects. Because of this, the effects of draw on the fiber microstructure were explored to understand the moduli trends shown in tensile testing data.

3.2 Crystal Structure

In semi-crystalline PAN polymer, random crystalline and amorphous regions provide contrasting properties. Crystalline regions represent the high strength and stiffness of the material, which when oriented in the direction of anticipated force result in a high modulus material [24]. The amorphous regions act as bonds between crystals and are free to relax at T_g ($\sim 125^\circ\text{C}$ for PAN) [9] to align under sufficient tensions [25]. During thermal conversion to carbon fibers, the crystal structure is rearranged completely as it is transformed to a fully amorphous material in stabilization and recrystallizes in carbonization [21]. The crystal structure of PAN precursor and carbon fiber was characterized and compared the draw in the following sections.

3.2.1 X-Ray Diffraction Test Methods

The structure and composition of the microstructure of polymer materials are commonly found using wide angle x-ray diffraction (WAXD). Continuing the investigation into the

processing/property/structure relationship of PAN precursor fiber, the following will detail the methods used to characterize the crystalline structure of the PAN precursor and resultant carbon fiber samples.

The effects of draw on specifically crystal size and orientation with the fiber axis was determined. Rigaku SmartLab X-ray diffraction system (Rigaku Corporation, Tokyo Japan) equipped with an $\alpha\beta$ -stage fiber sample attachment was used. Measurements were made using Ni-filtered $\text{CuK}\alpha$ ($\text{K}\alpha_1 + \text{K}\alpha_2$) radiation ($\text{K}\alpha_{1/2} = 0.497$, $\lambda = 1.542 \text{ \AA}$) at 40 kV and 44 mA. The fiber samples were analyzed about the equatorial and azimuthal directions for substance structure identification and arrangement respectively [40]. A schematic of the test angles is shown in figure 3.8.

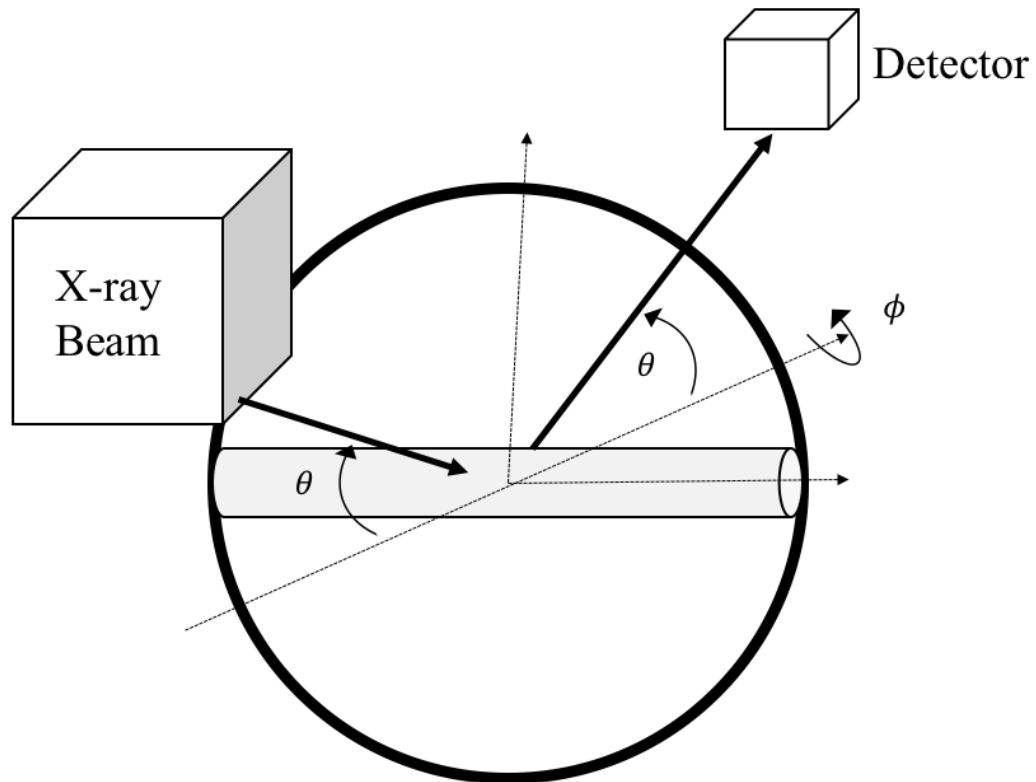


Figure 3.8 Schematic of the rotations in X-ray analysis of fiber.

In an equatorial scan, intensities are recorded as the x-ray beam and detector rotate (2θ) from the equatorial axis. In an azimuthal scan, the beam and detector are stationary at a

(2θ) Bragg angle and the fiber rotates about the azimuthal (ϕ). A full test procedure of the multi-step scans with test parameters is available in Appendix C.

A Theta/2Theta scan was performed about the equatorial direction to obtain the diffraction pattern and index the substance as semi-crystalline PAN having (100) and (110) planes [13] at $2\theta=16^\circ$ and 29° . The (100) planes were then investigated in an azimuthal scan, from which the peak shapes and intensities were used to determine the size and orientation of the crystalline regions with the axis of the fiber. Identical test formatting with slightly different parameters were used for identifying the diffraction pattern of carbon fiber containing planes (002) and (100) at $2\theta=25^\circ$ and 42° [41]. Peak intensities and diffraction data from azimuthal scans were fit using Gaussian functions and analyzed using the PDXL 2.0 software for crystal size and orientation calculations.

3.2.2 Hermans Orientation

The crystalline regions of the semi-crystalline PAN structure provide the material its strength. As these crystals align with the axis, the material becomes anisotropic with very high strengths in this direction. The following will focus on the calculation of the degree of preferred orientation of the crystalline regions of semi-crystalline PAN precursor and resultant carbon fiber.

To determine the uniaxial orientation of the crystals, azimuthal angle (ϕ) and intensities (I) from diffraction patterns about the axis scan of a known crystal plane (hkl) were used along with the equation for Hermans orientation factor (f) in equation 3.10.

$$f = \frac{3\langle \cos^2 \phi \rangle_{hkl} - 1}{2} \quad [3.10]$$

$$\langle \cos^2 \phi \rangle_{hkl} = \frac{\int_0^{\pi/2} I_{hkl}(\phi) \sin \phi \cos^2 \phi \, d\phi}{\int_0^{\pi/2} I_{hkl}(\phi) \sin \phi \, d\phi} \quad [3.11]$$

Where ϕ is the azimuthal angle between the fiber axis and the crystal axis and $I_{hkl}(\phi)$ is the intensity at that angle for the (hkl) Bragg peak. Intensities were measured from angles

-90° to 270°. A Hermans orientation factor of $f=1$ corresponds to crystal axes perfectly parallel with the fiber axis, for $f= -0.5$, the crystal axes are perpendicular with the fiber axis, and $f=0$ signifies that the crystal axes are randomly oriented [42].

3.2.3 Scherrer Equation

To explore how hot draw in solution spinning affects the dimensions of the crystals, the Scherrer equation is used to determine the crystallite thickness (L_c). Using the wavelength (λ) of the X-ray, the full width half maximum (FWHM) intensity of the peak (B), and shape factor (K), at Bragg angle (θ) corresponding to the peak of interest [21].

$$L_c = \frac{K\lambda}{B \cos \theta} \quad [3.12]$$

The angles (θ) corresponding to equatorial scan FWHM for PAN and carbon fiber at approximately $2\theta=16^\circ$ and $2\theta=25^\circ$ respectively were used to find crystal size. The instrumental shape factor and wavelength values used for these calculations were $K=0.94$ and $\lambda = 1.54 \text{ \AA}$. Crystal thickness of each WAXD tested sample was calculated using constant instrument and material parameters, FWHM values (B) and angles were obtained using the PDXL analysis software.

3.2.4 Results

Data from WAXD was used to determine the effects of draw on the characteristics of the crystal structure of PAN and resultant carbon fiber. WAXD azimuthal scans for PAN (a) precursor out of coagulation, (b) after hot draw, and (c) after thermal conversion to carbon fiber are compared in figure 3.9. The coagulation bath fiber has been stretched at low DDR in spin and gel draw. The figure shows the transformation of the very low orientation structure of coagulated fiber to the oriented semi-crystalline structure of hot drawn PAN precursor. As PAN precursor fiber is processed into carbon fiber, many changes occur in the microstructure and along with it, so do the fiber properties. Semi-crystalline PAN

precursor is converted to an amorphous structure in stabilization and recrystallizes independently from the precursor structure during carbonization [21]. These structural changes can be seen as the thin, high peaks of PAN precursor in (b) are transformed to short, wide peaks in (c) after thermal conversion to carbon fiber, indicating a drop in crystal orientation.

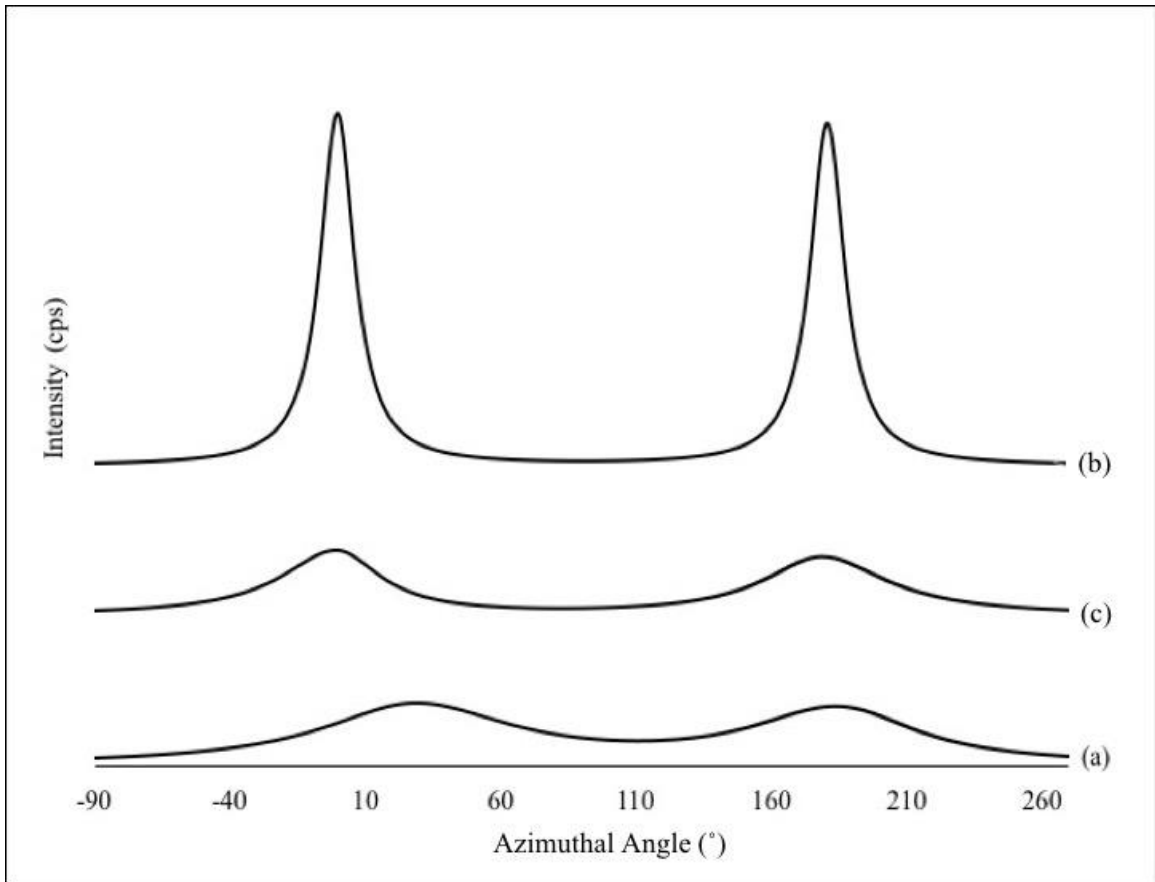


Figure 3.9. Azimuthal scans at (100) plane of PAN precursor fiber spin and gel drawn at $DDR= 1.52$, (b) combined spin, gel, and hot drawn at $DDR=1.52 \times 3.18=4.83$, (c) after thermal conversion to carbon fiber.

Table 3.4 Values for FWHM, crystal size (L_c), and Hermans orientation factor (f) for both PAN precursor and resultant carbon fibers for each DDR_{total} in hot draw during spinning.

WAXD Data						
DDR_{total}	PAN Precursor Fibers			Carbon Fibers		
	FWHM	L_c	Hermans Orientation Factor (f)	FWHM	L_c	Hermans Orientation Factor (f)
2.60	12.948	6.698	0.584	37.974	2.410	0.402
3.18	15.540	5.581	0.549	46.917	1.951	0.303
3.32	21.235	4.084	0.522	42.355	2.161	0.417
3.34	12.081	7.179	0.544	48.720	1.878	0.359
3.71	15.263	5.683	0.587	23.380	3.914	0.518
3.78	10.998	7.886	0.598	46.110	1.985	0.348
3.87	10.179	8.521	0.591	24.096	3.798	0.532
4.42	11.655	7.442	0.580	48.197	1.899	0.406
4.70	11.450	7.575	0.604	43.805	2.089	0.400
4.78	13.596	6.379	0.600	32.795	2.791	0.402
4.98	14.664	5.915	0.574			
5.19	11.024	7.868	0.587	35.783	2.558	0.423
5.20	11.650	7.445	0.610	26.832	3.411	0.442
5.24	12.945	6.700	0.602	23.845	3.838	0.464
5.66	20.070	4.321	0.590	26.450	3.460	0.466

WAXD data in table 3.4 shows a general increase in crystal size with increasing draw for PAN precursor and resultant carbon fibers. The relationships between draw and orientation are plotted in figures 3.10-3.11. PAN precursor shows a slight increase in orientation with draw, this increase is amplified after thermal conversion to carbon fiber shown in figure 3.10. The slight increase in PAN precursor orientation with draw quickly levels off to $f=0.6$, the lack of improvement past $DDR_{total}=3.5$ is indicative of a limit to the effects of hot draw during spinning on the orientation of the crystals. Also noticed, the trends seen in mechanical properties past the draw limit are not present here as crystal orientation is largely maintained and PAN precursor orientation tends to level off approaching the draw limit. Although crystalline orientation may show much improvement, other sections of the fiber, for example the amorphous regions in the structure may be improving in alignment. The changes in amorphous region orientations were not determined in this study because the characterization methods were specific to crystalline structure. Since the crystal orientation was only determined for fibers after hot draw, further study of the fibers subject

to gel and spin draw, prior to hot draw, is necessary to determine where crystal alignment is occurring and how much draw has an effect on this value.

PAN precursor orientation values are similar to the reported values for solution spun PAN precursor fibers of $f=0.66$ [43]. Carbon fiber orientations however, are lower than the reported values of high performance Toray PAN-based carbon fibers, $f=0.76-0.83$ [44]. These results suggest that in addition to draw during spinning, the thermal conversion process to carbon fiber significantly affects orientation of carbon fiber crystallites.

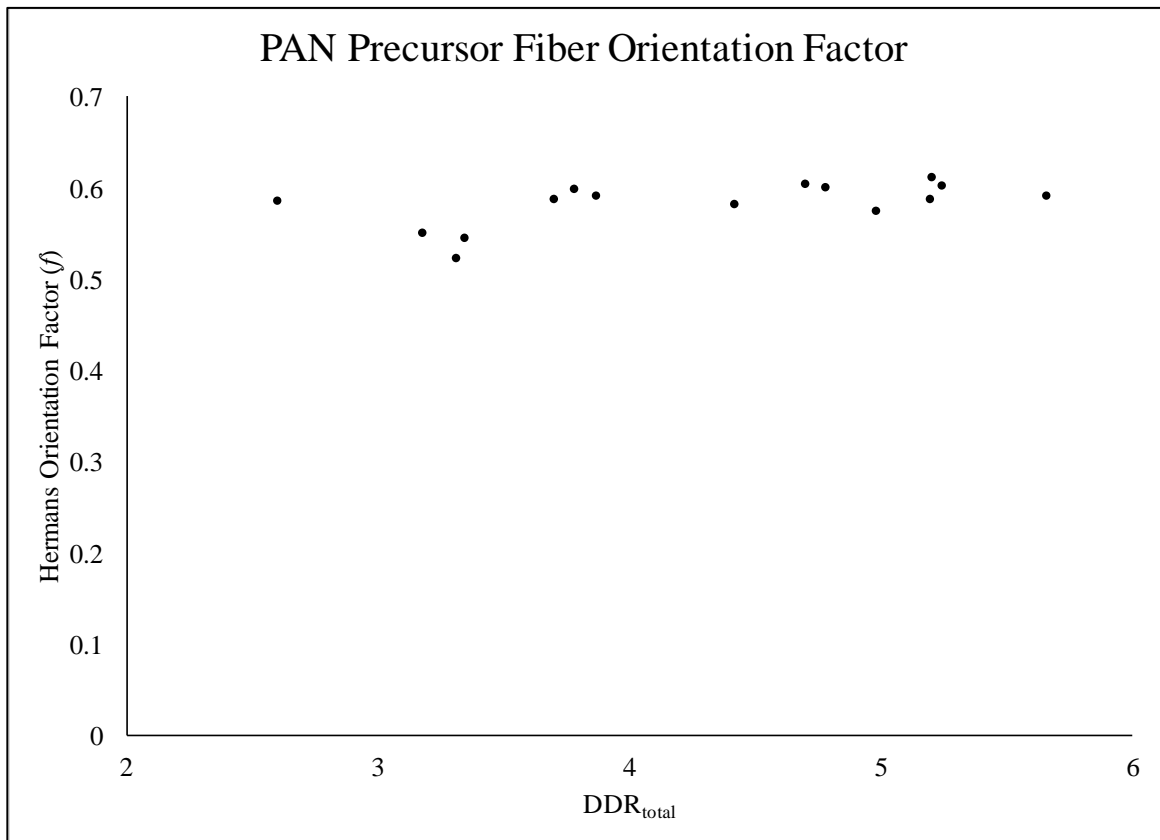


Figure 3.10 Calculated Hermans Orientation Factors for PAN precursor fiber vs. DDR_{total} .

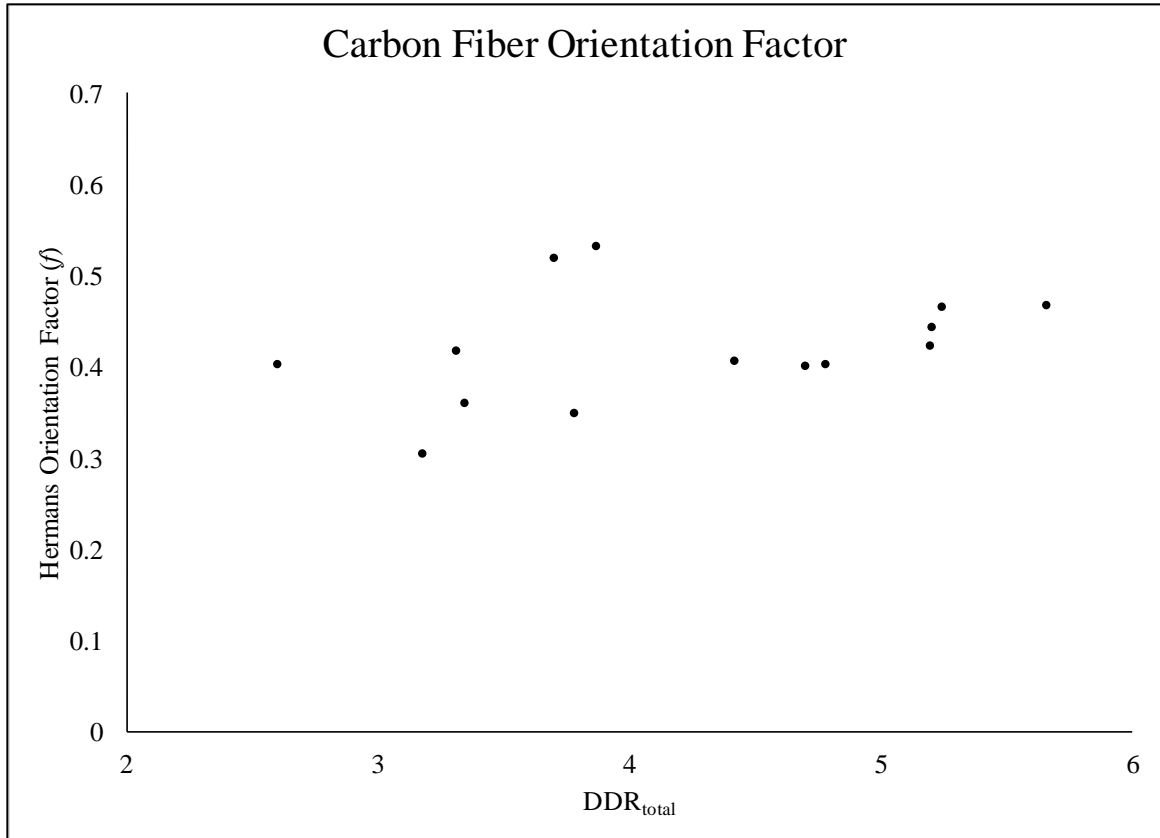


Figure 3.11 Calculated Hermans Orientation Factors for resultant carbon fiber vs. DDR_{total} .

3.3 Conclusion

PAN precursor fiber samples were collected while determining the limits to draw and then thermally converted to carbon fiber. The mechanical properties and microstructure of both PAN and resultant carbon fibers were analyzed at and below the determined draw limit. The goal of developing a processing/property/structure relationship of PAN precursor fiber and resultant carbon fiber was accomplished. The results of single filament tensile and XRD testing across a broad range of DDR revealed a correlation between modulus, break stress, and orientation to with increasing hot draw.

It was found that PAN precursor break stress and modulus values increased with increasing draw, reaching a maximum at the draw limit quantified as $DDR_{total} = 5.38 \pm 0.23$. At this limit, break stress and modulus values began to decrease and variation increased. The decreasing trend of PAN precursor properties after the draw limit was not carried through thermal conversion to carbon. Both break stress and modulus of carbon fibers continued to

increase with increasing draw past the draw limit. Weibull analysis of failure probability showed increasing Weibull modulus with draw to the same draw limit and a decrease after the draw limit was reached. This points to low numbers of defects right before the draw limit, after which the number of defects increases as indicated by break stress variation.

WAXD studies on PAN fiber and resultant carbon fiber show an increase in Hermans orientation factor with increasing draw. Approaching and exceeding the draw limit, these values continue to increase in carbon fiber, but begin to plateau in PAN precursor, suggesting maximum alignment capabilities earlier in PAN precursor draw.

The effects of draw on the mechanical performance and crystalline structure have been determined for PAN fiber and subsequent carbon fibers and the limits to draw have been quantified in this study. Results suggest there are limitations to draw on the improvement of modulus and break stress of PAN precursor fiber, but not resultant carbon fiber. Orientation with the fiber axis was seen to improve with draw for both PAN precursor and carbon fiber and a maximum orientation of PAN precursor was reached. Moreover, this study correlates the mechanical properties and crystal orientation of precursor and resultant carbon fiber to DDR_{total} during precursor spinning and determines its limitations. The resulting data from this experiment is specific to the Polyacrylonitrile polymer and spinning conditions used in this experiment. However, the fundamental relationships found pertaining to limits in multi-stage hot draw are expected to translate universally across changing PAN solution spinning parameters.

Chapter 4. Conclusion

This study uniquely quantified the limits of multi-stage hot draw in PAN precursor spinning and identified its effects on both PAN precursor fiber and the resultant carbon fiber. The essential control and understanding of processing conditions to produce a high-quality precursor material for carbon fiber was investigated in this study, the achievements and conclusions of this work are as follows.

Using the spinning capabilities at UK CAER, PAN precursor fiber conditions were systematically varied in first and second stage DDR to the point of unstable spinning conditions. The product of first and second stage hot draw limit at these instabilities was quantified as a single value of $DDR_{total}=5.38 \pm 0.23$, beyond which breaks in the line were expected to occur.

During PAN fiber spinning, there were many indications of poor processing conditions. In these experiments, observations were made and related to the conditions of the spinning. One observation made was the decline of fiber quality as filaments began to break, this was presented in the form of a “fuzzy” fiber. Tensions monitored during spinning were also recorded during these experiments. Tension values corresponding to breaks in second stage draw were determined to be 350 g-f. Maintaining tensions below this limit will reduce the presence of poor quality “fuzzy” fiber and improve handling characteristics for further processing and act as an additional way to quantify the limits of draw.

The properties of both PAN precursor and resultant carbon fiber, quantified by modulus (E) and break stress (σ) were determined for samples collected during the draw limit experiments. The microstructure of these materials was also studied in an attempt to provide a complete processing/structure/property relationship.

Using single filament tensile testing, the relationship between mechanical properties and draw of both PAN precursor and carbon fibers was determined. It was found for PAN precursor fiber that the improvement of mechanical properties associated with draw increase has a limit. Properties decline at and beyond the draw limit, where fiber spinning becomes unstable. Further, it was observed that after these fibers were converted to carbon fiber, improvement of mechanical properties continued to improve past the draw limit.

These findings suggest that while precursor fiber processing is very influential, it is not the only factor that affects resultant carbon fiber properties.

WAXD studies and Hermans orientation factor calculations determined that the orientation of the crystals in PAN precursor fiber showed a slight increase with increasing draw. These values remained level, as opposed to declining, after the draw limit. This indicated a maximum obtainable degree of orientation of $f=0.45$ with the axis in spinning. After thermal conversion, carbon fiber orientation showed greater improvement with increasing draw past the draw limit to a value of $f=0.60$.

The limitations of draw were found and quantified in this study using unique capabilities of in-house precursor fiber spinning. The actual samples of precursor gathered here were used to generate carbon fiber samples. By carefully studying these controlled, in-house processed fiber samples, the effects of draw on mechanical properties and microstructure of both parent precursor and resultant carbon fiber were found.

4.1 Future Work

The work done in this study has built a foundation to further study multi-stage draw processes during solution spinning of PAN precursor fiber. As research into this subject continues, additional study on the individual regions of draw is necessary to fully understand each component of multi-stage draw and how they combine to affect the fiber. Due to some of the conflicting results between PAN precursor and carbon fiber mechanical properties, further research and fine-tuning of temperature ramps and tension during thermal conversion is necessary to explore carbon fiber mechanical property and crystal orientation. Repeating these experiments and testing of collected samples from an improved carbonization method is required to obtain results of carbon fiber on par with industrial strength carbonization methods. To explain the lack of improvement of degree of crystal orientation with increasing draw and the potential of amorphous regions changing with draw, additional morphology characterization will be needed. A full study of the crystal and amorphous regions of fiber samples collected before and after every area of draw will determine the effects on all regions of the fiber microstructure. The results of these experiments and testing can produce a full timeline of the effects of draw on PAN

fiber during spinning and the resultant carbon fibers. This timeline can be used to show how crystals formed in coagulation align throughout the spinning process and also how the amorphous regions that link them are affected by draw. This study laid the ground work for many new studies on the numerous regions of draw during PAN solution spinning and their effects in an attempt to optimize draw conditions and the resulting carbon fibers.

APPENDICES

Appendix A: Derivation of diameter/draw down ratio relationship

Due to the conservation of mass and volume,

$$V_{in} = V_{out} \quad [A1]$$

modeling the fiber tow as a cylinder with cross sectional area (a) and length (l), A1 can be reworked as

$$[a * l]_{in} = [a * l]_{out} \quad [A2]$$

where the diameter (d) of the fiber tow, made up of hundreds to thousands of individual filaments.

$$a = \pi \frac{d^2}{4} \quad [A3]$$

Using the known definition of draw down ratio (DDR),

$$DDR = \frac{v_{in}}{v_{out}} \quad [A4]$$

where v represents the linear speed of the fiber entering and exiting the stretch stage in length (l) per time (t)

$$v = \frac{l}{t} \quad [A5]$$

DDR can be rewritten as the ratio of the length exiting (l_{out}) draw to the length entering (l_{in}) for a set amount of time (t), which then cancels out of the ratio to leave

$$DDR = \frac{l_{out}}{l_{in}} \quad [A6]$$

Combining A2, A3, and A6, DDR can be written in terms of cross sectional area, and thus diameter of the fiber tow.

$$\frac{a_{in}}{a_{out}} = \frac{d_{in}^2}{d_{out}^2} = \frac{l_{out}}{l_{in}} = DDR \quad [A7]$$

To find the diameter relationship before and after draw of single filaments, divide the d values above by the number of filaments expected in the tow.

Appendix B: Single Filament Tensile Testing Data

Tensile Testing Data									
PAN Precursor Fibers				Resultant Carbon Fibers					
DDR _{Total}	Diameter (μm)	Break Stress (MPa)	Modulus (GPa)	Diameter (μm)	Break Stress (MPa)	Modulus (GPa)	C _s	Corrected Modulus (GPa)	
2.60	9.67 1.31	744.27 121.48	16.33 2.79	5.69 0.30	1697.36 544.64	190.83 25.41	0.0002	195.69	26.44
3.18	10.33 0.67	652.62 57.30	15.02 0.69	6.51 0.33	1282.28 415.03	156.67 12.05	0.0003	163.86	13.07
3.32	9.30 0.71	685.11 42.50	14.63 0.80						
3.34	10.11 2.27	739.12 50.75	16.37 0.75						
3.71	8.92 0.24	755.50 53.30	15.04 0.60						
3.78	8.36 0.93	904.00 149.18	18.28 2.57	5.56 0.32	1705.25 400.07	192.90 11.72	0.0019	242.57	49.07
3.87	8.45 0.91	921.12 66.51	18.86 0.82						
4.42	7.98 1.74	886.61 244.25	19.08 3.56	4.88 0.39	1706.99 611.36	219.53 13.77	0.0006	233.25	26.51
4.70	7.15 0.46	754.36 251.95	18.22 2.48						
4.78	7.53 0.82	1000.05 174.51	20.68 1.34	4.72 0.24	2025.40 542.04	246.02 28.08	0.0003	254.48	29.39
4.98	8.44 1.05	942.35 148.03	19.14 1.44						
5.19	7.31 0.40	905.45 215.44	19.47 2.23						
5.20	7.57 1.01	756.28 276.09	15.69 4.40	4.55 0.27	1842.90 746.53	256.36 13.88	0.0003	265.10	14.10
5.24	7.36 1.08	830.98 251.53	18.07 2.20	4.43 0.32	2052.17 621.51	266.80 21.20	0.0003	275.88	21.05
5.66	7.13 0.62	981.58 176.95	15.47 3.53	4.46 0.22	2208.75 589.48	264.20 19.16	0.0004	276.05	19.05

Appendix C: Standard Operating Procedure for XRD Testing of PAN fiber

C.1 Purpose

The intent of this procedure is to outline the standard operating procedure for X-Ray Diffraction (XRD) analysis of PAN polymer fibers and resultant carbon fibers. These procedures will explain the steps for analysis using a Rigaku Smartlab XRD system.

C.2 Scope

The XRD data collected from these procedures are to be used in the study of the crystal structure of the fibers, specifically the alignment of crystals with the axis of the fiber. Two scans are performed in the process of obtaining this data. The initial Theta/2Theta scan provides information about the material's unit cells, information that can be used for material identification. After, a Phi scan is performed to further investigate an identifying plane of the crystal structure found during the Theta/2Theta scan.

C.3 Equipment

The following lists the equipment used in operation of this machine:

- Rigaku SmartLab X-Ray Diffractometer
- SC-70 Detector
- Cross Beam Optics (CBO) system
- Receiving Optical Device (ROD) adaptor unit
- Parallel-Beam (PB) selection 2 and 10 mm IS L slit
- 5 deg Soller/PSC
- Parallel-slit analyzer (PSA) Open and 0.114 deg
- Standard Z sample stage
- Height reference sample plate
- Alpha Beta Stage attachment
- Dial gage probe

- Ring sample holder
- Pinhole/clamp sample holder
- Allen wrench set for attachment change out

C.4 Sample Prep

It is very important when preparing a fiber sample for analysis using XRD, to ensure the following:

- Fibers are intact, no broken or loose filaments.
- Enough tension is applied to the fiber to remain taut but does not deform.
- Fiber tow is spread flat with no gaps between filaments.
- Fibers are parallel to one another, no crossing filaments.

One sample is needed for each of the two samples holders, one for each scan. The initial, theta/2theta scan will use a fiber ring as shown in top of figure C.4, the Phi scan will use a flat plate with a pinhole as shown in bottom of figure C.4. It is crucial that the fibers be mounted in the sample holders as similarly as possible.

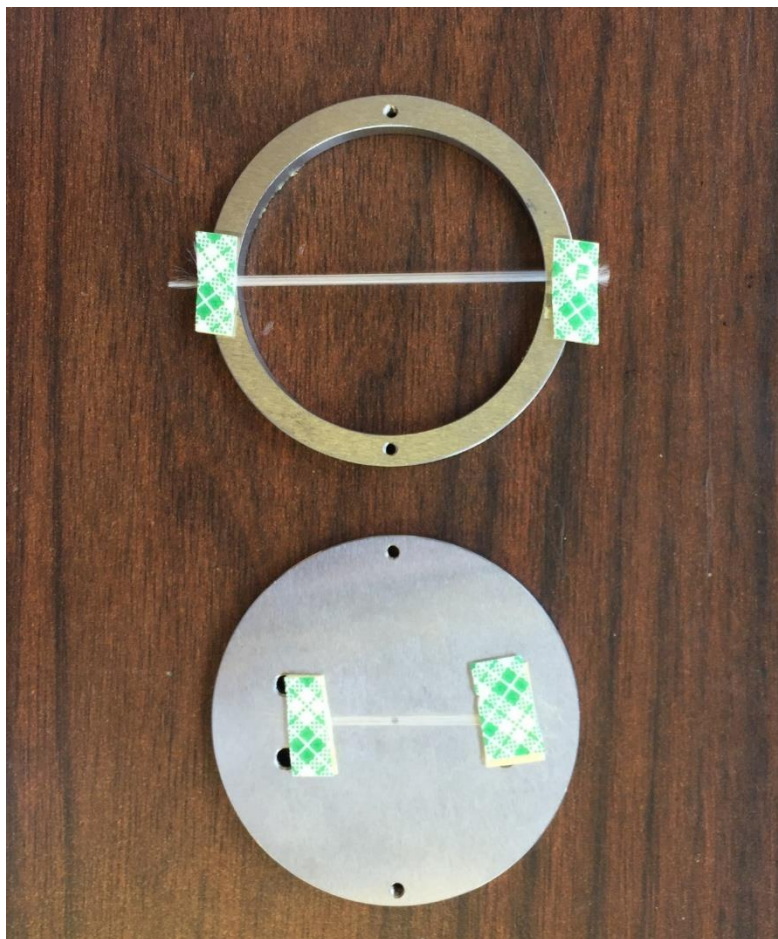


Figure C.4. PAN precursor sample mounts: Fiber ring sample holder for Phi scan (top),
Fiber flat plate sample holder for Theta/2Theta (bottom)

To mount a fiber sample onto the sample holder, cut a small length of fiber (~ 5") from the sample spool. Carefully do this, ensuring no filaments are tangled in the process and the tow remains smooth. Lie the fiber across the sample holder and spread it flat, avoiding gaps between filaments. Using two pieces of tape, secure the spread, flat tow along the parallel markings of the holder and trim the remaining fiber from the ends. Ensure that the fiber is mounted centered on the circular sample holder as shown in figure C.4 and that the flat plate sample holder pin hole is completely covered.

C.5. Start Up

Begin by selecting **Start up** and setting the Rigaku X-Ray parameters to the following:

Voltage: 45 kV

Current: 40 mA

then click **Execute** to initiate startup. Choose general med. resolution PB/PSA general as the measurement package to be used for these measurements.

C.6 Optics Alignment

Before fiber sample testing can begin, an optics alignment must be performed for the instrument. Run an optics alignment for the Rigaku using the standard Z stage attachment and center slit height reference sample plate as shown in figure C.6. This step is to ensure that the beam will be detected for the attachments used for the measurement through the sample. Optics alignment requires Open PSA and PSA 0.114 deg receiving optical devices (ROD adaptor) and 0.5 deg receiving parallel slit (RPS adaptor).

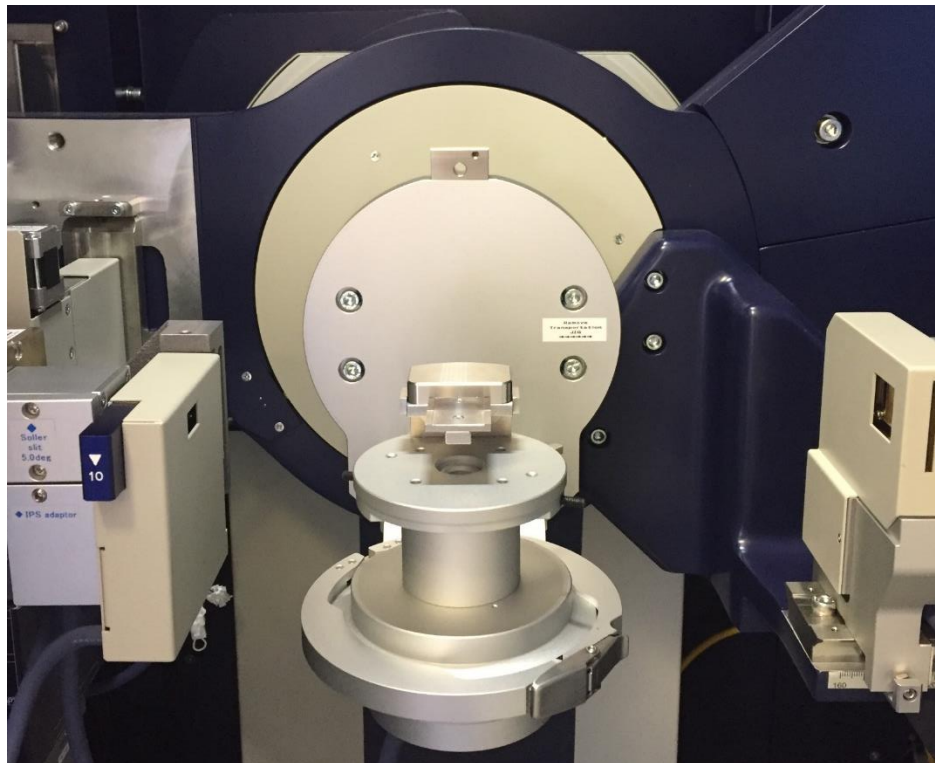


Figure C.6. Standard Z stage attachment with center slit height reference sample plate setup for optics alignment.

Select **Optics Alignment** and **Execute** and follow the guided instructions for the alignment, this will require a PSA change.

C.7.1 Z Scan Sample Alignment for Theta/2theta Scan

To start a sample alignment, replace the standard Z stage with the Alpha Beta stage attachment, manually adjust dial and flat reference to 0 and conduct a hardware configuration. Insert the fiber ring sample holder with sample into the stage with the axis of the fiber in line with 0° as shown in figure C.7. Turn the stage to transmission position for measurement.

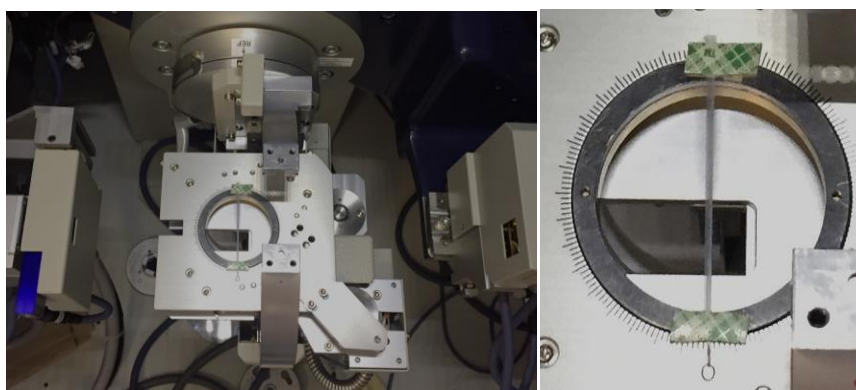


Figure C.7.1a Alpha Beta Stage attachment (left) and Fiber ring sample holder aligned with 0° marking on stage.

Using the Alpha Beta stage attachment for analysis of fiber samples requires manual alignment of the sample in the field of the X-Ray and detector plane. Using manual control, conduct a Z scan to find where the beam hits the fiber sample in the fiber ring sample holder. A Z scan should be performed before each Theta/2Theta and Phi scan as new samples are placed on the stage.

For fiber ring sample holder:

Insert the 10 mm beam length limiting slit.

In **Manual Control** settings

Theta/2theta= 0

Phi= 0

Z scan Start: -5 mm

Z scan Stop: 1.5 mm

Attenuator= 1/10000 or Auto

Perform a Z scan at the settings for a fiber ring sample holder, observe where the beam intensity drops as shown in figure C.7.1b, this will require using the zoom function to find the absolute lowest point. Record the x axis value (Z) of this drop as the z value for the Theta/2theta scan general measurement. Sample alignment is complete and instrument is ready for theta/2theta scan.

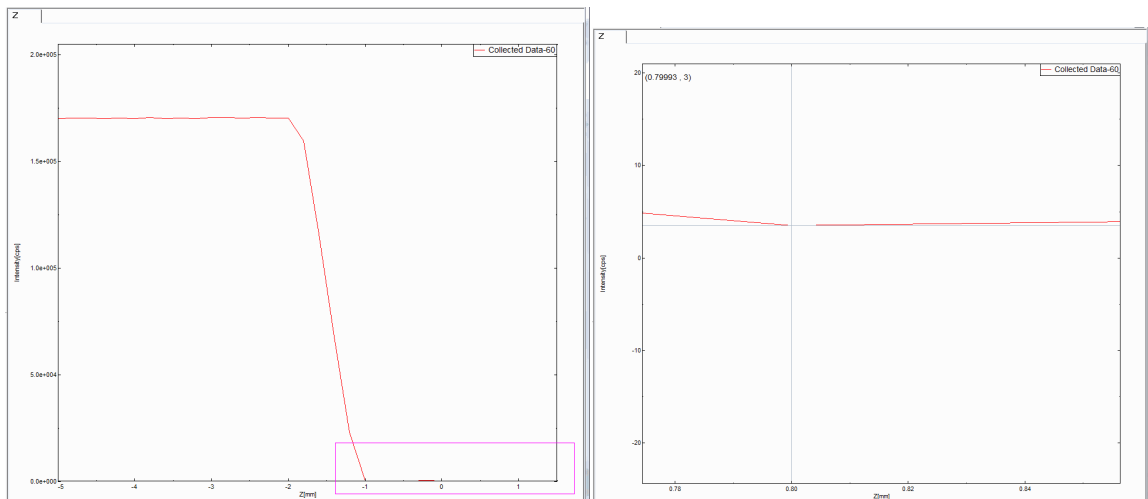


Figure C.7.1b Z scan of fiber ring sample alignment (left), zoomed image to find precise Z value (right).

Continue to C.8

C.7.2 Z Scan Sample Alignment for Phi Scan

For flat plate sample holder:

Insert the 2 mm beam length limiting slit.

Theta/2theta= 2θ value found in B.8 Theta/2Theta scan

Omega= $(1/2) \times 2\theta$ value found in B.8 Theta/2Theta scan

Z scan Start: -5 mm

Z scan Stop: 1.5 mm

Attenuator= Open

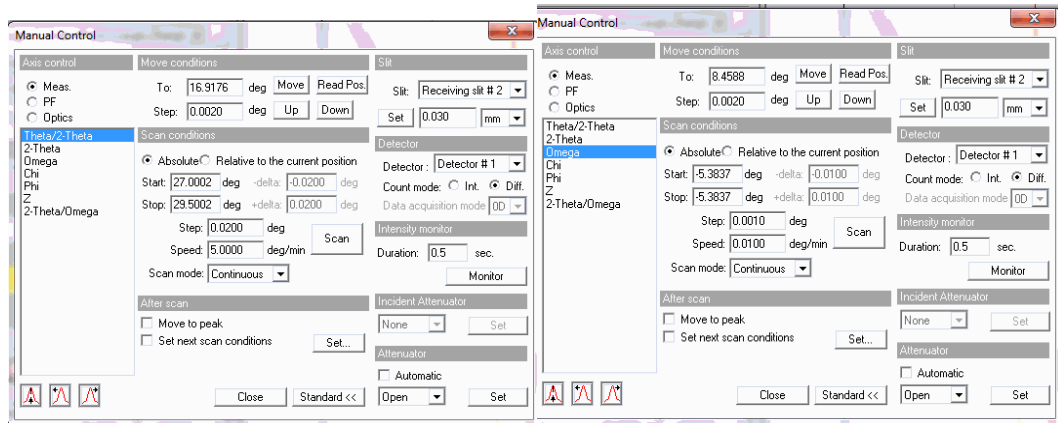


Figure C.7.2a. Z scan conditions found from Theta/2theta scan peaks.

Perform a Z scan at the settings for a fiber plate sample holder, observe where the beam intensity peaks as shown in figure C.7.2b, this will require using the zoom function to find the absolute highest point. Record the x axis (Z) value of this peak as the z value for the Phi scan general measurement. Sample alignment is complete and instrument is ready for Phi scan.

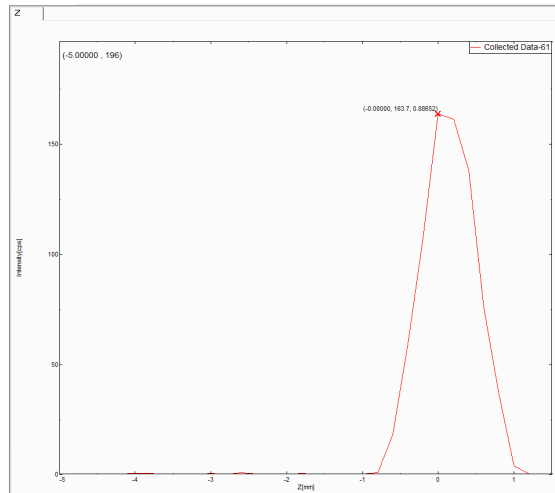


Figure C.7.2b. Z scan of fiber plate sample alignment

C.8 Theta/2Theta Scan

Ensure a hardware configuration has been performed. Select the **General Measurement** tab, enter file name, sample name, and any notes about the sample. Select **Read Current Slits** and ensure the conditions are as shown in figure C.8.1. Select **Set** and enter the z value obtained in C.7.1, select **Drive the 4 axes to current zero positions** box and **Execute** to begin Theta/2theta scan. When completed, a Theta/2theta scan for precursor fiber should resemble figure C.8.3, carbon fiber should resemble figure C.8.4. Find and record the x-axis Bragg angle (2θ) value at the first peak in the theta/2theta scan, representing the (100) planes and go back to C.7.2

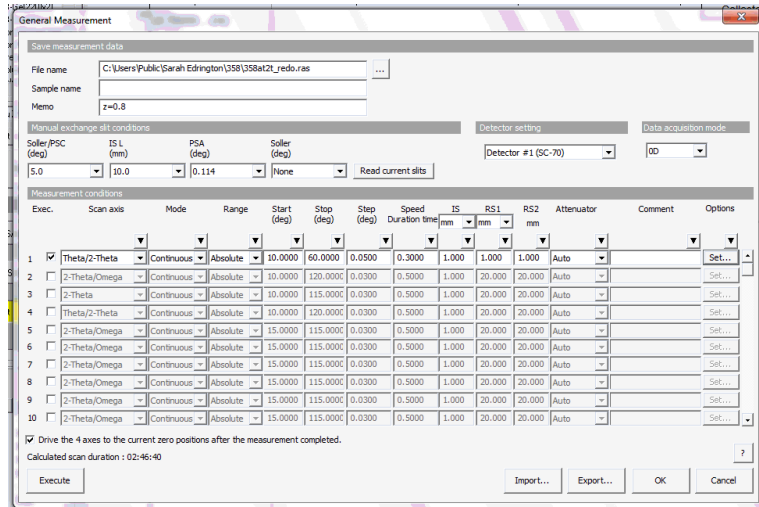


Figure C.8.1. General measurement conditions for Theta/2Theta scan

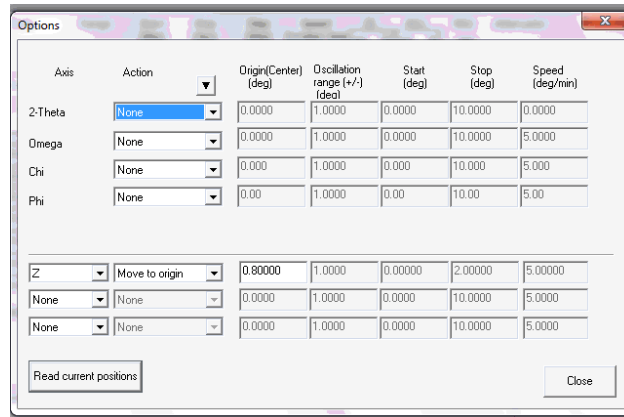


Figure C.8.2. Options for Theta/2Theta scan, enter recorded Z value from sample alignment Z scan C.7.1.

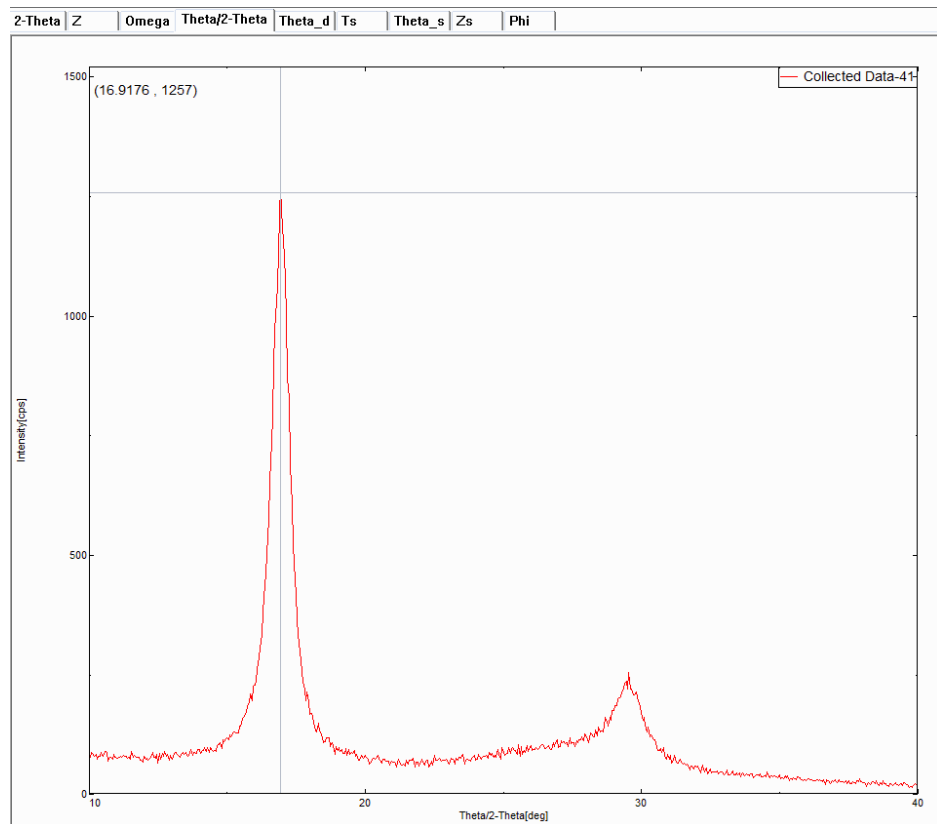


Figure C.8.3. Theta/2theta scan diffraction pattern of PAN fiber. First peak Bragg angle (2θ) values used for Phi scan conditions to investigate the (100) crystal plane.

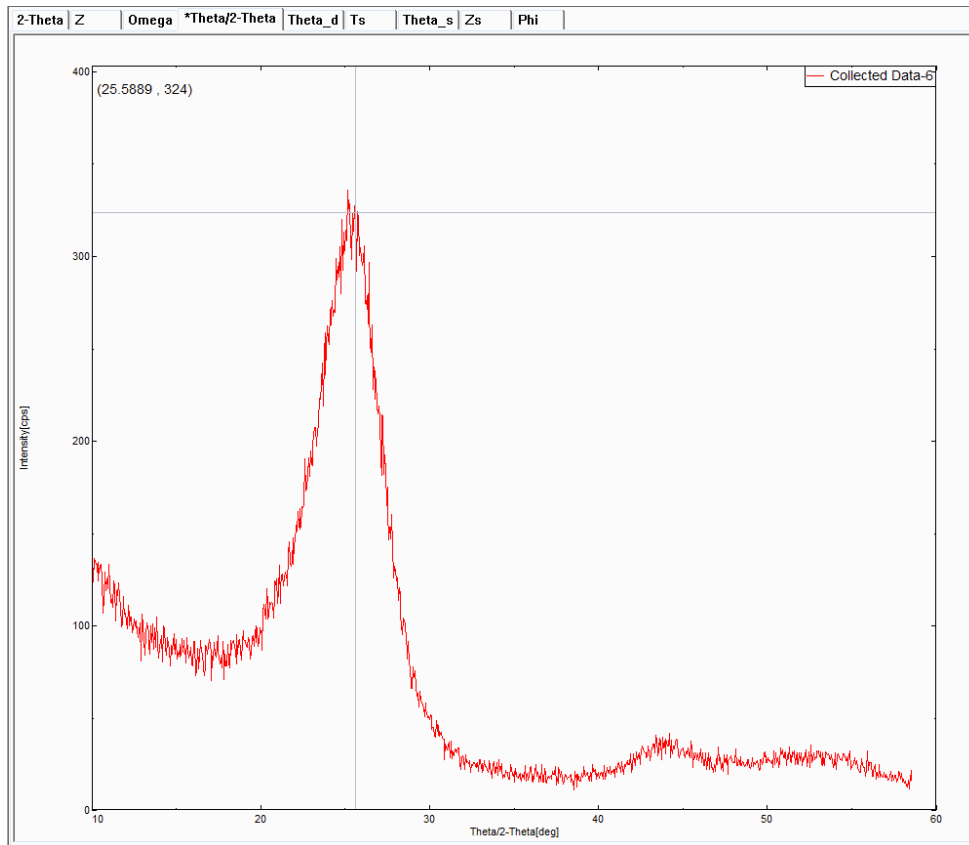


Figure C.8.4. Theta/2theta scan diffraction pattern of carbon fiber. First peak Bragg angle (2θ) value used for Phi scan conditions to investigate the (002) crystal plane.

C.9 Phi Scan

Replace the ring sample holder with the plate sample holder, mounting the fiber axis into the sample holder at 0° similarly done with the ring sample holder.

Perform a z scan using the flat plate sample holder conditions in C.7.2 and 2θ values found in C.8. Ensure a hardware configuration has been performed. Select the **General Measurement** tab, enter file name, sample name, and memo. Select **Read Current Slits** and ensure the conditions are as shown in figure C.9.1. Select **Set** and enter the Z value, Theta/2theta, and Omega values from C.7.2. Select **Drive the 4 axes to current zero positions** box and **Execute** to begin Phi scan.

General Measurement

Save measurement data

File name: C:\Users\Public\Sarah Edrington\358\358aphi_redo.ras

Sample name:

Memo: z=0.0

Manual exchange slit conditions: Soller/PSC (deg): 5.0, IS L (mm): 2.0, PSA (deg): 0.114, Soller (deg): None, Read current slits

Detector setting: Detector #1 (SC-70)

Data acquisition mode: 00

Measurement conditions

Exec.	Scan axis	Mode	Range	Start (deg)	Stop (deg)	Step (deg)	Speed Duration time	IS (mm)	RS1 (mm)	RS2 (mm)	Attenuator	Comment	Options
1	Phi	Continuous	Absolute	-90.00	260.00	0.20	8.00	1.000	20.000	20.000	Auto		Set...
2	2-Theta/Omega	Continuous	Absolute	10.0000	120.0000	0.0300	0.5000	1.000	20.000	20.000	Auto		Set...
3	2-Theta	Continuous	Absolute	10.0000	115.0000	0.0300	0.5000	1.000	20.000	20.000	Auto		Set...
4	Theta/2-Theta	Continuous	Absolute	10.0000	120.0000	0.0300	0.5000	1.000	20.000	20.000	Auto		Set...
5	2-Theta/Omega	Continuous	Absolute	15.0000	115.0000	0.0300	0.5000	1.000	20.000	20.000	Auto		Set...
6	2-Theta/Omega	Continuous	Absolute	15.0000	115.0000	0.0300	0.5000	1.000	20.000	20.000	Auto		Set...
7	2-Theta/Omega	Continuous	Absolute	15.0000	115.0000	0.0300	0.5000	1.000	20.000	20.000	Auto		Set...
8	2-Theta/Omega	Continuous	Absolute	15.0000	115.0000	0.0300	0.5000	1.000	20.000	20.000	Auto		Set...
9	2-Theta/Omega	Continuous	Absolute	15.0000	115.0000	0.0300	0.5000	1.000	20.000	20.000	Auto		Set...
10	2-Theta/Omega	Continuous	Absolute	15.0000	115.0000	0.0300	0.5000	1.000	20.000	20.000	Auto		Set...

Drive the 4 axes to the current zero positions after the measurement completed.

Calculated scan duration : 00:43:45

Execute Import... Export... OK Cancel

Figure C.9.1. General Measurement Conditions for Phi Scan

Options

Axis	Action	Origin(Center) (deg)	Oscillation range (+/-) (deg)	Start (deg)	Stop (deg)	Speed (deg/min)
2-Theta	Move to origin	16.9176	1.0000	0.0000	10.0000	0.0000
Omega	Move to origin	8.4588	1.0000	0.0000	10.0000	5.0000
Chi	None	0.0000	1.0000	0.0000	10.0000	5.0000
Phi	None	0.0000	1.0000	0.0000	10.0000	5.0000
Z	Move to origin	0.00000	1.0000	0.00000	2.00000	5.00000
None	None	0.00000	1.0000	0.00000	10.0000	5.00000
None	None	0.00000	1.0000	0.00000	10.0000	5.00000

Read current positions Close

Figure C.9.2. Options for Phi scan, enter recorded Theta/2Theta, Omega, and Z value from sample alignment Z scan.

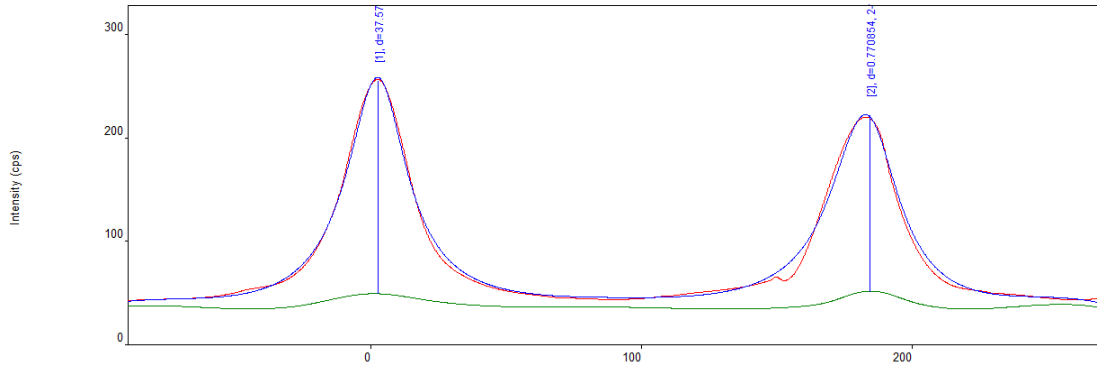


Figure C.9.3. Correct azimuthal (Phi) scan of a fiber sample.

A correct Phi scan about the azimuthal angle for both PAN precursor and carbon fiber is shown in figure C.9.3. To begin another test, return to step C.7.1.

C.10 Shutdown

Power down the instrument, select **Shut Down**, set

XG set: XG Off

Voltage: 20 kV

Current: 2 mA

And select **Execute**

REFERENCES

1. Warren, C.D., *Present and Future Automotive Composite Materials Research Efforts at DOE*. 12th International Conference on Composite Materials (ICCM-12), Paris, France, 1999.
2. *ASM Aerospace Specification Metals Inc.*. Available from: <http://asm.matweb.com/>.
3. Chand, C., *Review Carbon fibers for Composites*. Journal of Materials Science, 2000. **35**: p. 1303-1313.
4. Park, S.-J. and G.-Y. Heo, *Precursors and Manufacturing of Carbon Fibers*. 2015. **210**: p. 31-66.
5. Morgan, P., *Carbon fibers and their composites*. 2005, Boca Raton, LA: Taylor & Francis Group.
6. Hale, J., *Boeing 787 from the Ground Up*, in *Aero Magazine*.
7. *Carbon-Fiber Composites for Cars*, in *Oak Ridge National Laboratory Review*. 2000.
8. Mazumdar, D.S., *State of the Composites Industry*, in *Composite Manufacturing*. 2016.
9. Iversen, C.B., *Characterization of Polyacrylonitrile Carbon Fibers*. Biomedical and Chemical Engineering – eses, 2012.
10. Ribeiro, R.F.P., Luiz Claudio; ALVES, Nilton Pereira and BRITO JUNIOR, Carlos Alberto Rios *Thermal Stabilization study of polyacrylonitrile fiber obtained by extrusion*. Polímeros, 2015. **25**, 523-530 DOI: 10.1590/0104-1428.1938.
11. Song, Z., et al., *Enhancing Crystallinity and Orientation by Hot-Stretching to Improve the Mechanical Properties of Electrospun Partially Aligned Polyacrylonitrile (PAN) Nanocomposites*. Materials, 2011. **4**(12): p. 621-632.
12. Edie, D.D., *The Effect of Processing on the Structure and Properties of Carbon Fibers*. Carbon, 1998. **36**(4).
13. Anghelia, V.F., *Structural Analysis of PAN Fiber by X-Ray Diffraction*. Journal of Science and Arts, 2010. **1**(12): p. 89-94.
14. Salem, D.R., *Structure Formation in Polymeric Fibers*. 2001. p. 329-336.
15. Frank, E., D. Ingildeev, and M.R. Buchmeiser, *High-performance PAN-based carbon fibers and their performance requirements*, in *Structure and properties of high-performance fibers*, G. Bhat, Editor. 2017. p. 7-30.
16. Morris, E., M. Weisenberger, and G. Rice, *Properties of PAN Fibers Solution Spun into a Chilled Coagulation Bath at High Solvent Compositions*. Fibers, 2015. **3**(4): p. 560-574.
17. Lovell, R.J.Y.a.P.A., *Introduction to Polymers*. third ed. 2011, Boca Raton, FL: CRC Press.
18. Peterlin, A., *Drawing and extrusion of semi-crystalline polymers*. Colloid & Polymer Science, 1987. **265**(5): p. 357-382.
19. Agassant, J.-F., et al., *Polymer Processing: Principles and Modeling*, in *Polymer Processing: Principles and Modeling*. 1991. p. 228-230.
20. Su, J., et al., *A novel 3-D fabrication of platinum nanoparticles decorated micro carbon pillars electrode for high sensitivity detection of hydrogen peroxide*. Sensors and Actuators B: Chemical, 2013. **181**: p. 57-64.

21. Zhu, C.-z., et al., *2D SAXS/WAXD analysis of pan carbon fiber microstructure in organic/inorganic transformation*. Chinese Journal of Polymer Science, 2013. **31**(5): p. 823-832.
22. Dale Grove, P.D., and A. S. Abhiraman, *Exploratory Experiments in the Conversion of Plasticized Melt Spun PAN-Based Precursors to Carbon Fibers*. Carbon, 1988. **26**(3).
23. Newcomb, B.A., et al., *Processing, structure, and properties of gel spun PAN and PAN/CNT fibers and gel spun PAN based carbon fibers*. Polymer Engineering & Science, 2015. **55**(11): p. 2603-2614.
24. Xu, Q., et al., *A study on the orientation structure and mechanical properties of polyacrylonitrile precursors*. Polymers for Advanced Technologies, 2005. **16**(8): p. 642-645.
25. Chae, H.G., et al., *A comparison of reinforcement efficiency of various types of carbon nanotubes in polyacrylonitrile fiber*. Polymer, 2005. **46**(24): p. 10925-10935.
26. Lindenmeyer, P.H. and R. Hosemann, *Application of the Theory of Paracrystals to the Crystal Structure Analysis of Polyacrylonitrile*. Journal of Applied Physics, 1963. **34**(1): p. 42-45.
27. Rizzo, P., et al., *Conformational Disorder in the Pseudohexagonal Form of Atactic Polyacrylonitrile*. Macromolecules, 1996. **29**: p. 8852-8861.
28. Colvin, B.G., *The crystal structure of polyacrylonitrile*. European Polymer Journal, 1974. **10**: p. 337-340.
29. Qi-feng Qin, Y.-q.D., Kai Yi, Li Zhang, Ryu SeungKon and Ri-guang Jin, *Effects of Polymerization and Spinning Conditions on Mechanical Properties of PAN Precursor Fiber*. Carbon Letters, 2010. **11**(3).
30. Xiaomei Zeng, J.H., Jiongxin Zhao, Youwei Zhang, Ding Pan, *Investigation the jet stretch in the wet spinning of PAN fiber*. Journal of Applied Polymer Science, 1996. **59**(1).
31. Joh, Y., *Amorphous Polyacrylonitrile: Synthesis and Characterization*. Journal of Polymer Science: Polymer Chemistry Edition, 1979. **17**(12): p. 4051-4067.
32. Christian Wilms, G.S., Thomas Gries, *The Relationship between Process Technology, Structure Development and Fibre Properties in Modern Carbon Fibre Production*. Chemical Engineering Transactions, 2013. **32**.
33. Yu, M., et al., *Heredity and Difference of Multiple-Scale Microstructures in PAN-Based Carbon Fibers and Their Precursor Fibers*. Journal of Applied Polymer Science, 2012. **125**: p. 3159-3166.
34. Liu, X.D. and W. Ruland, *X-ray Studies on the Structure of Polyacrylonitrile Fibers*. Macromolecules, 1993. **26**(1993): p. 3030-3036.
35. Bell, J.P. and J.H. Dumbleton, *Changes in the Structure of Wet-Spun Acrylic Fibers During Processing*. Textile Research Journal, 1971. **41**: p. 196-203.
36. Sawai, D., Y. Fujii, and T. Kanamoto, *Development of oriented morphology and tensile properties upon superdrawing of solution-spun fibers of ultra-high molecular weight poly(acrylonitrile)*. Polymer, 2006. **47**(12): p. 4445-4453.
37. Gupta, B., et al., *Preparation of poly(lactic acid) fiber by dry-jet-wet-spinning. I. Influence of draw ratio on fiber properties*. Journal of Applied Polymer Science, 2006. **100**(2): p. 1239-1246.

38. Naito, K., et al., *The effect of gauge length on tensile strength and Weibull modulus of polyacrylonitrile (PAN)- and pitch-based carbon fibers*. Journal of Materials Science. **47**: p. 632-642.
39. S. Leroy, C.B., J.Perreau, , *Molecular Structure of an Electropolymerized Polyacrylonitrile Film and Its Pyrolyzed Deriatives*. 1984.
40. Cullity, B.D., *Elements of X-Ray Diffraction*. Second ed. Addison-Wesley Series in Metallurgy and Materials, ed. M. Cohen. 1978: Addison-Wesley Publishing Company, Inc.
41. N.S.Babu, *Structural and Morphological Features of Graphitised Carbon Fibers*. Trends in Applied Sciences Research, 2006. **1**(2): p. 204-213.
42. Yano, T., et al., *Orientation of poly(vinyl alcohol) nanofiber and crystallites in non-woven electrospun nanofiber mats under uniaxial stretching*. Polymer, 2012. **53**(21): p. 4702-4708.
43. Zussman, E., et al., *Mechanical and structural characterization of electrospun PAN-derived carbon nanofibers*. Carbon, 2005. **43**: p. 2175-2185.
44. Anderson, D.D.P., *Carbon Fiber Morphology, II: Expanded Wide-Angle X-Ray Diffraction Studies of Carbon Fibers*. 1991, University of Dayton Research Institute.

VITA

Name:

Sarah Elizabeth Edrington

Place of Birth:

Louisville, KY, USA

Education:

University of Kentucky

Bachelor of Science in Mechanical Engineering May 2015

Positions Held:

Undergraduate Research Assistant

Center for Applied Energy Research, University of Kentucky

September 2013-May 2015

Graduate Research Assistant

Center for Applied Energy Research, University of Kentucky

May 2015- May 2017

Publications:

Craddock, J. D., Burgess, J. J., Edrington, S. E., & Weisenberger, M. C. (2016). Method for Direct Measurement of On-Axis Carbon Fiber Thermal Diffusivity Using the Laser Flash Technique. *Journal of Thermal Science and Engineering Applications*, 9(1), 014502. doi:10.1115/1.4034853

Conferences and Presentations:

Edrington, S., Morris, E.A., Hochstrasser, N., Weisenberger, M.C., and Stewart, J. (2016, July). *PAN PRECURSOR DRAW AND STRAIN RATE DURING SPINNING: QUANTITATIVE EFFECTS ON MECHANICAL PROPERTIES AND ORIENTATION OF RESULTANT CARBON FIBER*. Paper presented at CARBON 2016, State College, Pennsylvania, USA.

Edrington, S., Morris, E.A., Hochstrasser, N., Weisenberger, M.C., and Stewart, J. (2016, September). *PAN Precursor Draw During Spinning: Effects on Mechanical Properties and Morphology of Resultant Carbon Fiber* Poster presented at the 2016 SPE Automotive Composites Conference & Exhibition, Detroit, MI.

Morris, E.A., Weisenberger, M.C., Edrington, S., (2015, April). *The Effects of Lignin Addition on the Properties of PAN-Based Carbon Fiber* Poster presented at The American Carbon Society Carbon Fibers and their composites Symposium/Workshop, Oak Ridge, TN.